MARVEL Analysis of the Measured High-resolution Rovibronic Spectra of $^{48}\text{Ti}^{16}\text{O}$

Laura K. McKemmish[1], Thomas Masseron[2], Samuel Sheppard[3], Elizabeth Sandeman[3], Zak Schofield[3], Tibor Furtenbacher[4], Attila G. Császár[4], Jonathan Tennyson[1], and Clara Sousa-Silva[1]

[1] Department of Physics and Astronomy, University College London, London, WC1E 6BT, UK; laura.mckemmish@gmail.com
[2] Institute of Astronomy, University of Cambridge, Madingley Road, Cambridge, CB3 0HA, UK
[3] Highams Park School, Handsworth Avenue, Highams Park, London, E4 9PJ, UK
[4] Institute of Chemistry, Eötvös Loránd University and MTA-ELTE Complex Chemical Systems Research Group, H-1518 Budapest 112, Hungary

Received 2016 September 30; revised 2016 December 22; accepted 2016 December 22; published 2017 February 8

Abstract

Accurate, experimental rovibronic energy levels, with associated labels and uncertainties, are reported for 11 low-lying electronic states of the diatomic $^{48}\text{Ti}^{16}\text{O}$ molecule, determined using the MARVEL (Measured Active Rotational-Vibrational Energy Levels) algorithm. All levels are based on lines corresponding to critically reviewed and validated high-resolution experimental spectra taken from 24 literature sources. The transition data are in the 2–22,160 cm^{-1} region. Out of the 49,679 measured transitions, 43,885 are triplet–triplet, 5710 are singlet–singlet, and 84 are triplet–singlet transitions. A careful analysis of the resulting experimental spectroscopic network (SN) allows 48,590 transitions to be validated. The transitions determine 93 vibrational band origins of $^{48}\text{Ti}^{16}\text{O}$, including 71 triplet and 22 singlet ones. There are 276 (73) triplet–triplet (singlet–singlet) band-heads derived from MARVEL experimental energies, 123(38) of which have never been assigned in low- or high-resolution experiments. The highest J value, where J stands for the total angular momentum, for which an energy level is validated is 163. The number of experimentally derived triplet and singlet $^{48}\text{Ti}^{16}\text{O}$ rovibrational energy levels is 8682 and 1882, respectively. The lists of validated lines and levels for $^{48}\text{Ti}^{16}\text{O}$ are deposited in the supporting information to this paper.

Key words: astronomical databases: miscellaneous – brown dwarfs – molecular data – opacity – planets and satellites: atmospheres – stars: low-mass

Supporting material: machine-readable table, tar.gz file

1. Introduction

Currently, any in-depth discussion on molecular data requirements, with astronomers working on cool stars or hot-Jupiter exoplanets, highlights one molecule: TiO (Hoeijmakers et al. 2015; Fortney et al. 2016; Tennyson et al. 2016b). TiO is the major near-infrared (IR) and visible absorber in M-type stars (Allard et al. 2000; Lodders 2002) and, potentially, hot-Jupiter exoplanets (Desert et al. 2008). Despite line lists from the late twentieth century generated by Collins (1975a), Collins & Fay (1976), Plez (1992), Jorgensen (1994), Schwenke (1998), and Plez (1998), and the recent VALD updates (Ryabchikova et al. 2015), the new very high-resolution observations, e.g., of exoplanetary atmospheres, cannot usually be modeled sufficiently accurately (Hoeijmakers et al. 2015).

Exoplanets provide two major topical applications of high-quality spectroscopic data for TiO.

First, detecting potentially habitable Earth-sized exoplanets using transits is expected to be easier around M-dwarf stars than other stellar hosts due to the higher transit depth and faster transit times. However, characterizing these planets requires high-accuracy modeling of M-dwarf stellar spectra, which is significantly complicated by the strong molecular absorption of these cooler stars (Allard et al. 1994, 2000). Compared to main-group closed-shell molecules like H_2O and CO, the spectra of transition metal diatomic species such as TiO and VO (McKemmish 2016b) are significantly less well determined

by either experimental or theoretical studies (Tennyson et al. 2016a). In particular, high-accuracy spectral modeling requires a thorough and accurate analysis of experimental data.

Second, TiO opacity is expected to be very important in modeling hot-Jupiter exoplanets without clouds (Fortney et al. 2008). However, due to the tidal interaction with their respective stars, there can be large differences in the day and night temperatures in hot Jupiters, giving rise to extreme conditions. This suggests that cloud cover is abundant on hot Jupiters, a supposition supported by observations (Nikolov et al. 2015; Sing et al. 2016). Thus far, studies of the presence of TiO in hot-Jupiter exoplanets have given mixed results. Evidence for TiO on WASP-121b was reported by Evans et al. (2016). The likely absence of TiO on WASP-19b was reported by Huitson et al. (2013) and on WASP-12b by Sing et al. (2013). It is predicted that the presence of TiO/VO in the atmospheres of hot-Jupiter exoplanets is likely to cause a thermal inversion in the atmosphere (Evans et al. 2016). Haynes et al. (2015) present an *HST* (*Hubble Space Telescope*) spectrum of WASP-33b consistent with emission from TiO. *HST* has been used to perform almost all of these observations; the upcoming launch of *JWST* (*James Webb Space Telescope*) will significantly increase the quality of the observed spectra. It is imperative to ensure that the quality of the available TiO line list is sufficiently high to allow these new spectra to be used optimally. Furthermore, the use of cross-correlation techniques allows ground-based telescopes to detect molecules (de Kok et al. 2014). The inaccuracies in current TiO line lists prevent the use of this technique for TiO (Hoeijmakers et al. 2015).

Table 1
Data Sources and Their Characteristics for $^{48}\text{Ti}^{16}\text{O}$, Including the Number of Measured (A) and Validated (V) Transitions (Trans.)

Tag	References			Range (cm⁻¹)	J Range	Trans. (A/V)	Uncertainties (cm⁻¹)			Comments
							Min	Av	Max	
50Phillips	Phillips (1950)	b $^1\Pi$–a $^1\Delta$	0–0	11106–11284	8–94	376/373	0.1	0.11	0.46	(1a)
		c $^1\Phi$–a $^1\Delta$	0–0	17761–17858	9–92	149/149	0.1	0.11	0.42	
50Phillips-ext	Phillips (1950)	c $^1\Phi$–a $^1\Delta$	0–0	17596–17860	2–101	178/178	0.2	0.2	0.2	(1a), (1d)
		c $^1\Phi$–a $^1\Delta$	1–1	17485–17760	2–100	283/207	0.2	0.24	0.55	
		c $^1\Phi$–a $^1\Delta$	2–2	17419–17654	2–100	252/182	0.2	0.25	0.55	
51Phillips	Phillips (1951)	A $^3\Phi$–X $^3\Delta$	0–0	13662–14172	5–119	765/763	0.1	0.11	0.49	(1a), (1b)
		A $^3\Phi$–X $^3\Delta$	0–1	12779–13173	8–95	642/632	0.1	0.11	0.48	
		A $^3\Phi$–X $^3\Delta$	1–0	14579–15031	6–90	638/635	0.1	0.11	0.51	
69Phillips	Phillips (1969)	B $^3\Pi$–X $^3\Delta$	0–0	16041–16233	2–61	340/340	0.1	0.11	0.39	(1a), (1c)
71PhDa	Phillips & Davis (1971)	e $^1\Sigma^+$–d $^1\Sigma^+$	0–0	24098–24302	1–50	80/78	0.05	0.051	0.075	(1a)
71Phillips	Phillips (1971)	B $^3\Pi$–X $^3\Delta$	0–0	16216–16259	0–36	192/138	0.1	0.24	0.53	(1a)
72Linton	Linton (1972)	f $^1\Delta$–a $^1\Delta$	0–0	18879–19076	2–66	111/109	0.05	0.074	0.19	(1e)
72Lindgren	Lindgren (1972)	e $^1\Sigma^+$–d $^1\Sigma^+$	1–0	24857–25147	8–60	91/91	0.05	0.053	0.11	(1f)
73Phillips	Phillips (1973)	A $^3\Phi$–X $^3\Delta$	0–0	13365–14172	2–171	1353/1353	0.2	0.2	0.42	(1a), (1d)
		A $^3\Phi$–X $^3\Delta$	0–1	12340–13173	1–162	1276/1276	0.2	0.2	0.52	
		A $^3\Phi$–X $^3\Delta$	0–2	11696–12183	2–120	800/795	0.2	0.2	0.48	
		A $^3\Phi$–X $^3\Delta$	1–0	14140–15031	1–158	1263/1262	0.2	0.2	0.28	
		A $^3\Phi$–X $^3\Delta$	1–1	13177–14031	1–165	1308/1308	0.2	0.2	0.34	
		A $^3\Phi$–X $^3\Delta$	1–2	12456–13041	1–143	1099/1097	0.2	0.2	0.46	
		A $^3\Phi$–X $^3\Delta$	1–3	11527–12061	1–151	1000/984	0.2	0.2	0.55	
		A $^3\Phi$–X $^3\Delta$	2–0	14994–15882	1–164	1230/1227	0.2	0.21	0.51	
		A $^3\Phi$–X $^3\Delta$	2–1	13952–14882	1–149	1211/1207	0.2	0.2	0.5	
		A $^3\Phi$–X $^3\Delta$	2–3	12237–12911	1–148	1107/1103	0.2	0.2	0.54	
		A $^3\Phi$–X $^3\Delta$	2–4	11524–11940	1–125	838/795	0.2	0.2	0.51	
		A $^3\Phi$–X $^3\Delta$	3–1	14991–15725	1–147	1056/1053	0.2	0.21	0.4	
		A $^3\Phi$–X $^3\Delta$	3–2	13909–14735	1–151	1104/1099	0.2	0.2	0.36	
		A $^3\Phi$–X $^3\Delta$	3–4	12237–12782	1–131	908/891	0.2	0.2	0.4	
		A $^3\Phi$–X $^3\Delta$	3–5	11494–11820	1–125	868/833	0.2	0.2	0.34	
		A $^3\Phi$–X $^3\Delta$	4–2	14813–15570	1–136	1062/1049	0.2	0.2	0.42	
		A $^3\Phi$–X $^3\Delta$	4–3	13761–14589	1–149	1051/1038	0.2	0.21	0.5	
		A $^3\Phi$–X $^3\Delta$	4–5	12041–12655	1–134	991/973	0.2	0.2	0.4	
		A $^3\Phi$–X $^3\Delta$	5–3	14781–15417	2–136	1025/1016	0.2	0.2	0.4	
		B $^3\Pi$–X $^3\Delta$	0–0	15560–16259	1–141	1735/1560	0.2	0.21	0.52	
		C $^3\Delta$–X $^3\Delta$	0–0	18298–19349	1–159	879/879	0.2	0.2	0.27	
		C $^3\Delta$–X $^3\Delta$	0–1	17327–18349	1–157	864/864	0.2	0.2	0.48	
		C $^3\Delta$–X $^3\Delta$	0–2	16661–17359	1–143	689/686	0.2	0.2	0.48	
		C $^3\Delta$–X $^3\Delta$	0–3	15929–16378	2–100	438/411	0.2	0.21	0.53	
		C $^3\Delta$–X $^3\Delta$	1–0	18926–20178	1–156	848/842	0.2	0.2	0.27	
		C $^3\Delta$–X $^3\Delta$	1–2	17369–18188	1–126	706/698	0.2	0.2	0.47	
		C $^3\Delta$–X $^3\Delta$	1–3	16660–17206	1–118	629/586	0.2	0.21	0.53	
		C $^3\Delta$–X $^3\Delta$	2–0	20292–20998	1–107	609/608	0.2	0.2	0.35	
		C $^3\Delta$–X $^3\Delta$	2–1	19081–19998	1–126	637/637	0.2	0.2	0.38	
		C $^3\Delta$–X $^3\Delta$	2–3	17707–18026	1–88	346/343	0.2	0.21	0.54	
		C $^3\Delta$–X $^3\Delta$	2–4	16427–17054	1–112	536/512	0.2	0.21	0.54	
		C $^3\Delta$–X $^3\Delta$	3–0	21191–21809	1–111	584/582	0.2	0.2	0.35	
		C $^3\Delta$–X $^3\Delta$	3–1	19976–20809	2–120	630/622	0.2	0.2	0.54	
		C $^3\Delta$–X $^3\Delta$	3–5	16444–16902	1–117	464/445	0.2	0.21	0.51	
		C $^3\Delta$–X $^3\Delta$	4–0	22089–22610	1–101	456/444	0.2	0.2	0.38	
		C $^3\Delta$–X $^3\Delta$	4–1	20896–21611	1–105	509/497	0.2	0.2	0.25	
		C $^3\Delta$–X $^3\Delta$	4–2	20260–20620	2–90	439/430	0.2	0.2	0.35	
		C $^3\Delta$–X $^3\Delta$	5–1	21898–22404	2–83	361/358	0.2	0.2	0.51	
		C $^3\Delta$–X $^3\Delta$	5–2	20830–21414	2–92	381/379	0.2	0.2	0.51	
		C $^3\Delta$–X $^3\Delta$	6–2	21794–22195	3–73	321/319	0.2	0.2	0.33	
		C $^3\Delta$–X $^3\Delta$	6–3	20847–21214	4–86	276/270	0.2	0.2	0.44	
		C $^3\Delta$–X $^3\Delta$	7–3	21654–21986	1–67	293/293	0.2	0.2	0.2	
74LiSi	Linton & Singhal (1974)	b $^1\Pi$–a $^1\Delta$	0–0	11198–11284	1–43	158/158	0.1	0.1	0.36	

Table 1
(Continued)

Tag	References			Range (cm^{-1})	J Range	Trans. (A/V)	Uncertainties (cm^{-1}) Min	Av	Max	Comments
74Linton	Linton (1974)	c $^1\Phi$–a $^1\Delta$	0–0	17715–17859	2–74	189/189	0.02	0.035	0.13	
		c $^1\Phi$–a $^1\Delta$	1–1	17634–17759	2–72	177/169	0.02	0.023	0.09	
		c $^1\Phi$–a $^1\Delta$	2–2	17523–17658	2–67	162/161	0.02	0.023	0.1	
		c $^1\Phi$–a $^1\Delta$	3–3	17443–17556	2–69	152/152	0.02	0.022	0.056	
79HoGeMe	Hocking et al. (1979)	B $^3\Pi$–X $^3\Delta$	0–0	15951–16259	1–55	732/731	0.008	0.013	0.087	(1g)
		B $^3\Pi$–X $^3\Delta$	0–1	15002–15245	0–50	586/586	0.008	0.011	0.043	
		B $^3\Pi$–X $^3\Delta$	1–0	16862–17122	1–56	664/602	0.008	0.0095	0.064	
		B $^3\Pi$–X $^3\Delta$	1–1	15835–16107	1–55	546/367	0.008	0.014	0.093	
79GaDe	Gallaher & DeVore (1979)	X $^3\Delta$–X $^3\Delta$	1–0	975–1022	2–22	40/40	0.2	0.2	0.3	(1h)
80GaBrDa	Galehouse et al. (1980)	b $^1\Pi$–d $^1\Sigma^+$	0–0	8775–9062	1–93	240/240	0.01	0.011	0.074	
		b $^1\Pi$–d $^1\Sigma^+$	0–1	7757–8049	0–86	210/210	0.01	0.011	0.041	
		b $^1\Pi$–d $^1\Sigma^+$	0–2	6952–7046	7–49	49/49	0.01	0.01	0.014	
		b $^1\Pi$–d $^1\Sigma^+$	1–0	9598–9972	0–86	233/233	0.01	0.016	0.32	
		b $^1\Pi$–d $^1\Sigma^+$	1–1	8773–8960	0–70	152/152	0.01	0.012	0.078	
		b $^1\Pi$–d $^1\Sigma^+$	1–2	7758–7957	2–77	174/174	0.01	0.015	0.11	
		b $^1\Pi$–d $^1\Sigma^+$	1–3	6826–6964	1–67	95/95	0.01	0.013	0.084	
		b $^1\Pi$–d $^1\Sigma^+$	2–0	10712–10874	1–60	123/123	0.01	0.017	0.34	
		b $^1\Pi$–d $^1\Sigma^+$	2–1	9582–9862	0–72	171/171	0.01	0.011	0.05	
		b $^1\Pi$–d $^1\Sigma^+$	2–3	7679–7866	1–75	117/117	0.01	0.011	0.028	
		b $^1\Pi$–d $^1\Sigma^+$	3–1	10446–10755	0–74	151/151	0.01	0.015	0.096	
		b $^1\Pi$–d $^1\Sigma^+$	3–2	9558–9708	46–70	34/34	0.01	0.019	0.073	
		b $^1\Pi$–d $^1\Sigma^+$	3–4	7646–7776	0–51	95/95	0.01	0.014	0.17	
		b $^1\Pi$–d $^1\Sigma^+$	3–5	6708–6802	2–55	43/43	0.01	0.01	0.01	
		b $^1\Pi$–d $^1\Sigma^+$	4–2	10397–10636	0–66	153/153	0.01	0.015	0.094	
		b $^1\Pi$–d $^1\Sigma^+$	4–3	9626–9643	1–32	32/32	0.01	0.013	0.035	
85BrGa	Brandes & Galehouse (1985)	f $^1\Delta$–a $^1\Delta$	0–0	18830–19077	2–71	127/127	0.044	0.044	0.056	
		f $^1\Delta$–a $^1\Delta$	0–1	17841–18068	2–69	116/116	0.044	0.045	0.1	
		f $^1\Delta$–a $^1\Delta$	1–0	19726–19945	2–63	101/101	0.044	0.044	0.057	
		f $^1\Delta$–a $^1\Delta$	1–1	18744–18937	2–60	93/93	0.044	0.045	0.081	
		f $^1\Delta$–a $^1\Delta$	1–2	17774–17937	3–56	67/67	0.044	0.046	0.13	
		f $^1\Delta$–a $^1\Delta$	2–1	19748–19800	4–24	27/27	0.044	0.044	0.044	
90StShJuRu	Steimle et al. (1990)	X $^3\Delta$–X $^3\Delta$	0–0	2–3	1–3	2/2	10^{-5}	10^{-5}	10^{-5}	(1i)
91GuAmVe	Gustavsson et al. (1991)	B $^3\Pi$–X $^3\Delta$	1–2	14848–15134	3–48	171/170	0.03	0.031	0.046	(1j)
		B $^3\Pi$–X $^3\Delta$	1–3	13925–14129	6–24	14/14	0.03	0.031	0.05	
		C $^3\Delta$–X $^3\Delta$	2–1	19930–19995	5–23	9/9	0.03	0.036	0.061	
		C $^3\Delta$–X $^3\Delta$	2–2	18946–18992	15–21	7/7	0.03	0.03	0.03	
		C $^3\Delta$–X $^3\Delta$	2–4	16965–17040	10–31	23/23	0.03	0.031	0.06	
		C $^3\Delta$–X $^3\Delta$	2–5	16031–16088	5–22	24/24	0.03	0.03	0.03	
91SiHa	Simard & Hackett (1991)	E $^3\Pi$–X $^3\Delta$	0–0	11801–11852	0–15	111/109	0.1	0.13	0.47	
95KaMcHe	Kaledin et al. (1995)	C $^3\Delta$–a $^1\Delta$	2–0	17675–17738	2–34	84/84	0.01	0.013	0.089	
		C $^3\Delta$–X $^3\Delta$	2–3	17969–18011	3–26	42/42	0.01	0.014	0.045	
		C $^3\Delta$–X $^3\Delta$	2–4	16995–17040	3–27	39/39	0.01	0.01	0.019	
96AmChLu	Amiot et al. (1996)	c $^1\Phi$–a $^1\Delta$	0–0	17711–17860	3–97	114/114	0.005	0.0052	0.0091	(1k)
96BaMeMe	Barnes et al. (1996)	A $^3\Phi$–X $^3\Delta$	0–0	14022–14172	1–26	63/63	0.0002	0.0003	0.00063	
96RaBeWa	Ram et al. (1996)	b $^1\Pi$–a $^1\Delta$	0–0	10960–11284	1–108	405/404	0.02	0.021	0.076	
		b $^1\Pi$–a $^1\Delta$	1–1	11009–11186	1–82	231/231	0.02	0.021	0.05	
98NaSaRoSt	Namiki et al. (1998)	X $^3\Delta$–X $^3\Delta$	0–0	7–12	6–11	9/9	10^{-7}	10^{-7}	10^{-7}	(1l)

Table 1
(Continued)

Tag	References			Range (cm^{-1})	J Range	Trans. (A/V)	Uncertainties (cm^{-1})			Comments
							Min	Av	Max	
99RaBeDuWa	Ram et al. (1999)									(1m)
-Lab		A $^3\Phi$–X $^3\Delta$	0–0	13863–14172	3–89	291/285	0.004	0.0044	0.02	
		A $^3\Phi$–X $^3\Delta$	0–1	12918–13173	3–66	368/355	0.004	0.0054	0.09	
		A $^3\Phi$–X $^3\Delta$	1–0	14725–15031	2–72	243/239	0.004	0.0047	0.023	
		A $^3\Phi$–X $^3\Delta$	1–1	13729–14031	3–72	409/392	0.004	0.0047	0.026	
		A $^3\Phi$–X $^3\Delta$	1–2	12809–13041	2–68	382/377	0.004	0.0049	0.031	
		A $^3\Phi$–X $^3\Delta$	2–1	14592–14882	5–66	360/354	0.004	0.0049	0.022	
		A $^3\Phi$–X $^3\Delta$	2–3	12680–12911	3–54	268/267	0.004	0.0046	0.017	
		A $^3\Phi$–X $^3\Delta$	3–2	14478–14733	4–59	241/241	0.004	0.0044	0.022	
		A $^3\Phi$–X $^3\Delta$	3–4	12588–12760	7–52	138/137	0.004	0.0042	0.012	
		A $^3\Phi$–X $^3\Delta$	4–3	14336–14589	8–59	244/243	0.004	0.0043	0.012	
-Sunspots (SS)		A $^3\Phi$–X $^3\Delta$	0–0	13601–14071	30–110	132/132	0.01	0.01	0.03	
		A $^3\Phi$–X $^3\Delta$	0–1	12830–13123	11–98	102/102	0.01	0.012	0.044	
		A $^3\Phi$–X $^3\Delta$	1–0	14673–14883	12–83	57/57	0.01	0.012	0.043	
		A $^3\Phi$–X $^3\Delta$	1–1	13606–13936	26–107	94/94	0.01	0.011	0.033	
		A $^3\Phi$–X $^3\Delta$	1–2	12703–12958	11–98	149/149	0.01	0.011	0.046	
		A $^3\Phi$–X $^3\Delta$	2–1	14671–14722	7–66	4/4	0.01	0.019	0.038	
		A $^3\Phi$–X $^3\Delta$	2–2	13618–13817	16–82	70/70	0.01	0.012	0.042	
		A $^3\Phi$–X $^3\Delta$	2–3	12660–12831	13–83	77/76	0.01	0.011	0.027	
02KoHaMuSe	Kobayashi et al. (2002)	A $^3\Phi$–X $^3\Delta$	0–2	12176–12182	3–15	12/12	0.01	0.016	0.025	(1n)
		E $^3\Pi$–X $^3\Delta$	0–0	11796–11855	0–35	348/347	0.01	0.01	0.036	
		E $^3\Pi$–X $^3\Delta$	1–0	12739–12760	0–13	57/56	0.01	0.01	0.024	

Note. See Section 2.5 for comments.
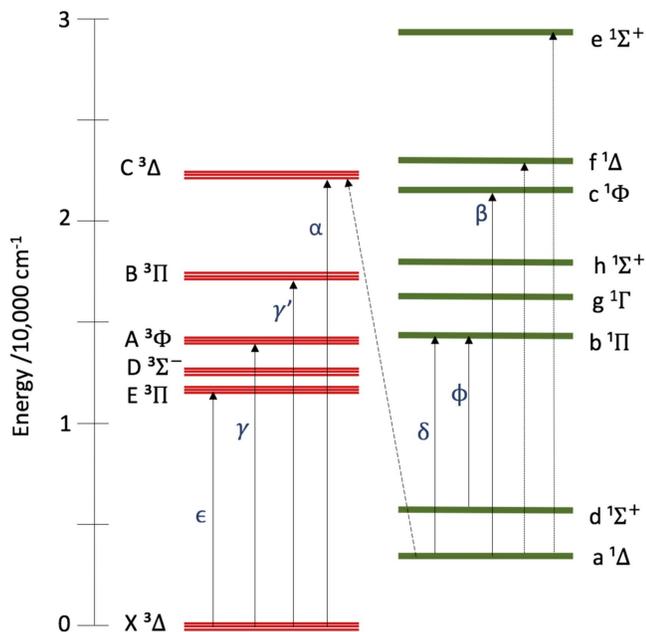
Figure 1. Band system of ^{48}Ti^{16}O showing the bands considered in this work. The long-dashed line represents an experimentally observed intercombination band. The short-dashed lines represent experimentally observed transitions that have not been named. There are three fine-structure components for the triplet Π, Δ, and Φ states (for the ground electronic state, X $^3\Delta_1$ is the lowest-energy component).

Historically, the detection of TiO in M-giants by Fowler (1904) was one of the earliest molecular detections in stellar astrophysics, predating modern quantum mechanics. The very high experimental interest in this, from a chemical perspective, unusual molecule over the last century, as documented thoroughly in this manuscript (Tables 1 and 3–5, see below), is a direct consequence of this early identification in stellar bodies. TiO, together with C$_2$ (Furtenbacher et al. 2016), has provided a major motivating factor for the development of theory and methods in the field of rovibronic spectroscopy. The references collated in this paper tell a fascinating story of how scientists tackled the complexity of transition metal diatomic spectra without significant computational power and thus without accurate ab initio predictions. Questions like whether the singlet or triplet state was the true ground state did not have obvious answers. The triplet ground state was misidentified twice (Lowater 1929; Phillips 1951) before finally being assigned correctly as X $^3\Delta$ by Phillips (1969). The dominant electronic configuration of the X $^3\Delta$ ground electronic state can be written as (core)$(9\sigma)^1(1\delta)^1$, where 9σ and 1δ are essentially the $4s$ and $3d$ orbitals of Ti^{2+}, respectively. The singlet–triplet gap was estimated, e.g., by Phillips (1952), then eventually measured using formally spin-forbidden transitions first by Kobylyansky et al. (1983) and then more accurately by Kaledin et al. (1995). This manuscript considers and collates all the available and assigned TiO experimental spectroscopic frequency data. We then use the Measured Active Rotational-Vibrational Energy Levels (MARVEL) algorithm (Császár et al. 2007; Furtenbacher et al. 2007; Furtenbacher & Császár 2012b), described in detail below, to extract the highest accuracy collation of TiO rovibronic energy levels ever produced. The experimentally derived energy levels are all given uncertainties. The MARVEL procedure is active in that future experimental data can be added to the collation and used

Table 2
Extract from the 48Ti-16O.marvel.inp Input File for ^{48}Ti^{16}O

1	2	3	4	5	6	7	8	9
$\tilde{\nu}$	$\Delta\tilde{\nu}$	State$'$	J'	v'	State$''$	J''	v''	ID
14463.63	0.2	A3Phi_3	122	1	X3Delta_2	122	0	73Phillips_AX.18910
14336.8	0.2	A3Phi_3	122	1	X3Delta_2	123	0	73Phillips_AX.18914
14634.87	0.2	A3Phi_4	122	1	X3Delta_3	121	0	73Phillips_AX.18916
14508.26	0.2	A3Phi_4	122	1	X3Delta_3	122	0	73Phillips_AX.18918
14380.56	0.2	A3Phi_4	122	1	X3Delta_3	123	0	73Phillips_AX.18922
14408.6	0.2	A3Phi_2	123	1	X3Delta_1	123	0	73Phillips_AX.19008
14281.54	0.2	A3Phi_2	123	1	X3Delta_1	124	0	73Phillips_AX.19010
14582.06	0.2	A3Phi_3	123	1	X3Delta_2	122	0	73Phillips_AX.19012
9635.433	0.01	b1Pi	3f	4	d1Sigma+	3	3	80GaBrDa.65
9640.637	0.012	b1Pi	22e	4	d1Sigma+	21	3	80GaBrDa.662
9637.572	0.015	b1Pi	26e	4	d1Sigma+	25	3	80GaBrDa.802
9639.478	0.033	b1Pi	4e	4	d1Sigma+	3	3	80GaBrDa.85
9635.617	0.01	b1Pi	28e	4	d1Sigma+	27	3	80GaBrDa.868
9635.162	0.01	b1Pi	4f	4	d1Sigma+	4	3	80GaBrDa.97
16229.687	0.127596	B3Pi_0	5b	0	X3Delta_1	4	0	69Phxxxx.1
16231.492	0.213806	B3Pi_0	14b	0	X3Delta_1	13	0	69Phxxxx.10
16197.913	0.1	B3Pi_0	46a	0	X3Delta_1	45	0	69Phxxxx.100
16195.911	0.1	B3Pi_0	47a	0	X3Delta_1	46	0	69Phxxxx.101
16193.918	0.1	B3Pi_0	48a	0	X3Delta_1	47	0	69Phxxxx.102
16191.766	0.1	B3Pi_0	49a	0	X3Delta_1	48	0	69Phxxxx.103
16189.615	0.1	B3Pi_0	50a	0	X3Delta_1	49	0	69Phxxxx.104

Column	Notation	
1	$\tilde{\nu}$	Transition wavenumber (in cm^{-1})
2	$\Delta\tilde{\nu}$	Estimated uncertainty in transition wavenumber (in cm^{-1})
3	State$'$	Electronic state of upper energy level, including Ω for triplet states, where $\Omega = \Lambda + \Sigma$; Λ and Σ are projections of the total angular momentum and the electron spin angular momentum on the internuclear axis, respectively, of the upper level
4	J'	Total angular momentum of upper level and rotationaless parity for Π states
5	v'	Vibrational quantum number of upper level
6	State$''$	Electronic state of lower energy level, including Ω for triplet states
7	J''	Total angular momentum of lower level and rotationaless parity for Π states
8	v''	Vibrational quantum number of lower level
9	ID	Unique ID for transition, with reference key for source (see Table 1) and counting number

(This table is available in its entirety in FITS format.)

to produce updated experimentally derived energy levels in a straightforward manner. These energy levels can be substituted into line lists to improve their quality (McKemmish et al. 2016b; Barber et al. 2014; Paulose et al. 2015).

2. Theory

2.1. MARVEL

The MARVEL approach (Császár et al. 2007; Furtenbacher et al. 2007; Furtenbacher & Császár 2012b) is a sophisticated methodology that allows the extraction of experimental energy levels, and associated uncertainties, from a (usually large) set of experimental transition frequencies. The methodology is similar to traditional approaches based on the Ritz principle, such as "combination differences," but is a more sophisticated, computational, near-black-box approach. The MARVEL program takes formatted assigned transitions as input. The program then constructs the experimental spectroscopic networks (SNs) (Császár & Furtenbacher 2011; Furtenbacher & Császár 2012a; Furtenbacher et al. 2014; Árendás et al. 2016; Császár et al. 2016), which contain all inter-connected transitions. For each SN, the assigned transition data is then inverted to find the energy levels. The uncertainties of the transition frequencies weight this

inversion process using a robust reweighting procedure advocated by Watson (2003), allowing MARVEL to yield the uncertainty of each extracted energy level. For a detailed description of the approach, algorithm, and program, we refer readers to Furtenbacher & Császár (2012b). MARVEL was originally developed and used by an IUPAC Task Group (TG) studying water spectra (Tennyson et al. 2014a) and applied to various water isotopologues (Tennyson et al. 2009, 2010, 2013, 2014b). The energy levels these studies yielded will provide the major source of water transition frequencies in the upcoming 2016 update of HITRAN (I. E. Gordon et al. 2017, in preparation). The naming convention for data sources employed here follows the one proposed by this IUPAC TG. Other molecules for which rovibrational energy levels have been determined using MARVEL include H_3^+ (Furtenbacher et al. 2013b), $H_2^{12}C^{12}C^{16}O$ (Fábri et al. 2011), H_2D^+ and D_2H^+ (Furtenbacher et al. 2013a), and $^{14}NH_3$ (Al Derzi et al. 2015). The only previous use of MARVEL for rovibronic spectra is the recently published analysis of $^{12}C_2$ (Furtenbacher et al. 2016).

The MARVEL software takes as input assigned, measured transitions, with estimated uncertainties, and outputs assigned energy levels together with recommended uncertainties. However, there is often no consistent set of energy levels that

Table 3
TiO References That Contain Experimental Measurements of Band Positions
(Often Band-heads)

Tag	References	System	#	Comment
28Lowater	Lowater (1928)	various, some unassigned	144	(3a)
29Christya	Christy (1929a)	A-X, C-X	62	(3b)
37WuMe	Wurm & Meister (1937)	b-a, b-d	7	(3a)
57GaRoJu	Gatterer et al. (1957)	b-a	1	(3a)
69LiNi	Linton & Nicholls (1969)	c-a	4	(3a)
69Lockwood	Lockwood (1969)	b-d, b-a	7	
69Phillips	Phillips (1969)	B-X	32	
72PhDa	Phillips & Davis (1972)	C-X	22	(3c)
76ZyPa	Zyrnicki & Palmer (1976)	B-X	20	
77LiBrb	Linton & Broida (1977b)	E-X	45	(3c)
82DeVore	DeVore (1982)	f-a	8	

Note. See Section 2.6 for comments. # Refers to the number of band-heads provided.

produce the input transitions within the estimated uncertainties. This can occur due to typographic or digitization errors, mis-assignments, and under-estimated uncertainties for the transitions. For this reason, the master list of MARVEL input transitions should be gradually increased with issues resolved as new transitions are added to the master file. MARVEL produces new recommended uncertainties for the transitions. If these are less than twice the original uncertainties, we generally adopt these recommended uncertainties. If there is a very large difference in the recommended uncertainty, we look for typographic and digitization errors; if none are found, we then assume mis-assignment and put a negative in front of the transition wavenumber, thus retaining the datum but not utilizing it in the MARVEL algorithm for future runs. Transitions initially discarded in this way can be reconsidered later in the process. For each band in each experimental source, we track the number of validated transitions (i.e., transitions for which all extracted energies of the full data set are consistent) against the number of total input transitions as well as the minimum, average and maximum uncertainty of transition frequencies. The minimum uncertainty is usually our initial input uncertainty based on the original experimental paper (or our best educated guess) because the current MARVEL code can automatically increase uncertainties but not reduce them. Generally, if we find that the average uncertainty is significantly higher than the minimum uncertainty, we increase the minimum uncertainty of the whole data set, and rerun the MARVEL analysis.

It is important throughout, and particularly at the final stage, that the trends and patterns in the energy levels are validated using available means. In previous studies, this has often been done against energies calculated theoretically; here we are more reliant on trends such as a reasonably systematic quadratic increase in energy with J, an approximately linear increase with vibrational quantum number, and so forth. Some of us are also part-way through constructing a spectroscopic model of TiO using the DUO software (Yurchenko et al. 2016); this also

Table 4
TiO References That Contain Measurements Relevant to the Verification of the
Dipole Moments, e.g., Lifetimes, Transition Intensities (Relative or Absolute),
and Dipole Moment Measurements

Tag	References	Type	Bands/States
54Phillips	Phillips (1954)	Relative intensity	C-X
70LiNi	Linton & Nicholls (1970)	Relative intensity	C-X, c-a
71PrSuPe	Price et al. (1971)	Intensity	A-X, C-X
72Dube	Dube (1972)	Intensity	c-a
74PrSuPe	Price et al. (1974)	Intensity	A-X, C-X
74FaWoBe	Fairbair et al. (1974)	Intensity	C-X
75Zyrnicki	Zyrnicki (1975)	Intensity	c-a
76FeBiDa	Feinberg et al. (1976)	Lifetime	c $^1\Phi$ ($v = 0$)
77FeDa	Feinberg & Davis (1977)	Lifetime	c $^1\Phi$ ($v = 0$)
78FeDa	Feinberg & Davis (1978)	Lifetime	C $^3\Delta_3$ ($v = 2$, $J = 17, 87$)
78StLi	Steele & Linton (1978)	Lifetime	C $^3\Delta$ ($v = 0, 1, 2$)
79RaRaRa	Rao et al. (1979)	Intensity	B-X
86DaLiPh	Davis et al. (1986)	Intensity	c-a, b-a, b-d, B-X, A-X and C-X
89StSh	Steimle & Shirley (1989)	Dipole moment	X
92CaSc	Carette & Schamps (1992)	Lifetime	B $^3\Pi_1$ ($v = 0$)
92DoWe	Doverstal & Weijnitz (1992)	Lifetime	A $^3\Phi_2$ ($v = 0$), B $^3\Pi_0$ ($v = 0$), C $^3\Delta_1$ ($v = 0$)
95HeNaCo	Hedgecock et al. (1995)	Lifetime	A, B, C, c, f and E
98Lundevall	Lundevall (1998)	Lifetime	E $^3\Pi$ ($v = 0$)
03StVi	Steimle & Virgo (2003)	Dipole moment	X, E, A and B
03NaMiIt	Namiki et al. (2003b)	Intensity	C-X
04NaSaIt	Namiki et al. (2004)	Intensity	C-X

allowed a preliminary validation of energy levels against a realistic theoretical model.

2.2. Electronic Structure and Spectroscopy of TiO

Like other transition-metal-containing diatomic species, TiO has a large number of low-lying electronic states, which contribute significantly to the level density of the recorded spectra in the near-IR and in the visible. Those states with excitation energies below $23{,}000\,\mathrm{cm}^{-1}$, and other well-characterized experimental electronic states are shown in Figure 1, which also gives the observed bands linking these states. The triplet ground state has allowed excitations to the E $^3\Pi$, A $^3\Phi$, B $^3\Pi$, and C $^3\Delta$ states. At the temperatures of the planetary atmospheres where TiO is thought to be abundant (i.e., 1500 to 3000 K), significant absorption also occurs from

Table 5
TiO References That Are Not Used in the Rotationally Resolved MARVEL or Band-head Analysis and Do Not Focus on Intensity Determination

Tag	References	Comment
1904Fowler	Fowler (1904)	No explicit assignment
26King	King (1926)	No rotationally resolved data
27BiCh	Birge & Christy (1927)	Paper not available online
28ChBi	Christy & Birge (1928)	No rotationally resolved data
29Lowater	Lowater (1929)	No absolute band position data
29Christyb	Christy (1929b)	Summary of 29Christya
36Budo	Budo (1936)	Combination differences only
37Dobron	Dobronravin (1937)	Source not available, but the measurements are unlikely to be accurate enough for use
52Phillips	Phillips (1952)	Identification of ground state symmetry, no new data
59Pettera	Pettersson (1959b)	Source not available, but the measurements are unlikely to be accurate enough for use in MARVEL
59Petterb	Pettersson (1959a)	Source not available, but the measurements are unlikely to be accurate enough for use in MARVEL
61PeLi	Pettersson & Lindgren (1961)	Figures only, no numerical data
62Petter	Pettersson & Lindgren (1962)	Source not available, but the measurements are unlikely to be accurate enough to use in MARVEL; contains d-b data
68Makita	Makita (1968)	sunspot data with 63 lines only
70PaPa	Pathak & Palmer (1970)	Band-heads only, and very high energy bands considered
71McThWe	McIntyre et al. (1971)	Inert neon matrix used, band-heads only
72BaGuPiDe	Balducci et al. (1972)	Dissociation energy only
72PaHs	Palmer & Hsu (1972)	Band-heads only in UV
73Engvold	Engvold (1973)	Fitting to sunspot spectral, newer data available
74Phillips	Phillips (1974)	Prediction of X $^3\Delta$ energy levels based on combination differences of other observed data
75BrBr	Brom & Broida (1975)	Inert neon matrix used, band-heads only
75Collins	Collins (1975b)	Analysis only
76Hilden	Hildenbrand (1976)	No spectroscopic data, only dissociation energy
77DuGo	Dubois & Gole (1977)	No rotationally resolved data; band-heads for highly excited state only
77LiBra	Linton & Broida (1977a)	Original measurement of C-a transition frequency, no tabulated rotationally resolved data
83KoKuGu	Kobylyansky et al. (1983)	Measurement of singlet-triplet energy gap
84DyGrJoLe	Dyke et al. (1984)	Limited data on band-heads that is available elsewhere
85CaCrDu	Carlson et al. (1985)	No relevant data
93FlScJu	Fletcher et al. (1993)	Analysis of hyperfine structure in $^{47}Ti^{16}O$
94WiRoVa	Williamson et al. (1994)	Transitions observed in inert argon matrix
95AmAzLu	Amiot et al. (1995)	Original transition data unfortunately not found: B-X (1,0) band at high

Table 5
(Continued)

Tag	References	Comment
		sub-Doppler resolution (0.002 cm^{-1}) up to J = 96 according to paper
97BaMeMe	Barnes et al. (1997)	Contains bands from very high $^3\Pi$ electronic states that give evidence of D $^3\Sigma^-$ state at 12 284 cm^{-1} above X $^3\Delta$, with a vibrational frequency around 968 cm^{-1}
97LudAAmVe	Luc et al. (1997)	Reanalysis of data from 96AmChLu
98VeLuAm	Vetter et al. (1998)	Reanalysis of data from 96AmChLu and 95AmAzLu
00CoSiGl	Colibaba-Evulet et al. (2000)	Low-resolution data demonstrating detection only
01HePeDu	Hermann et al. (2001)	Unassigned very high temperature spectra
02AmLuVe	Amiot et al. (2002)	No data on the $^{48}Ti^{16}O$ isotopologue
03NaItDa	Namiki et al. (2003a)	No new experimental data
05ViStBr	Virgo et al. (2005)	Zeeman splitting data only, B-X (0-0) and A-X (0-0)
12WoPaHo	Woods et al. (2012)	Unresolved spectra
13HuLuChLa	Huang et al. (2013)	TiO$^+$ spectra, some low-resolution TiO bands not considered here

Note. This list concentrates on sunspot observations analyzed specifically for TiO, experimental studies or analyses of experimental studies.

the thermal population of the a $^1\Delta$ and d $^1\Sigma^+$ states to higher singlet states, b $^1\Pi$, c $^1\Phi$, f $^1\Delta$, and e $^1\Sigma^+$.

2.3. Quantum Numbers and Selection Rules

MARVEL uses quantum numbers solely as part of the labels used to uniquely identify each rovibronic state and the corresponding energy level. The three most obvious descriptors to use for the rovibronic states of TiO are the electronic state, *state*, the total angular momentum quantum number, *J*, and the vibrational quantum number, *v*. We find these descriptors to be relatively unambiguous, despite the fact that the vibrational quantum numbers are not good quantum numbers. For the triplet energy levels, we further need to give information about the coupling of the electronic angular momenta; we choose to do this in the Hund's coupling case (a) formulation (Bernath 2016). For Hund's coupling case (a), the Ω quantum number is the sum of the quantum numbers describing the axial component of the electron orbital angular momentum *L*, Λ, and that of the electron spin angular momentum *S*, Σ, *i.e.*, $\Omega = \Lambda + \Sigma$. Coupling case (a) is a good representation whenever $A\Lambda$ is much greater than BJ, where A (which can be both positive and negative) is the spin–orbit coupling constant and B is the rotational constant. For the X $^3\Delta$ ground electronic state of TiO $A = 50.7$ cm^{-1}; thus, of the three fine-structure components $^3\Delta_\Omega$ the lowest state is $^3\Delta_1$. Transitions within all three fine-structure states have been observed experimentally (Table 6, *vide infra*). Note that Hund's coupling case (a) becomes less appropriate as *J* increases (in this study, energy levels with rather large *J* values occur). For singlet states, the component of the total electronic angular momentum
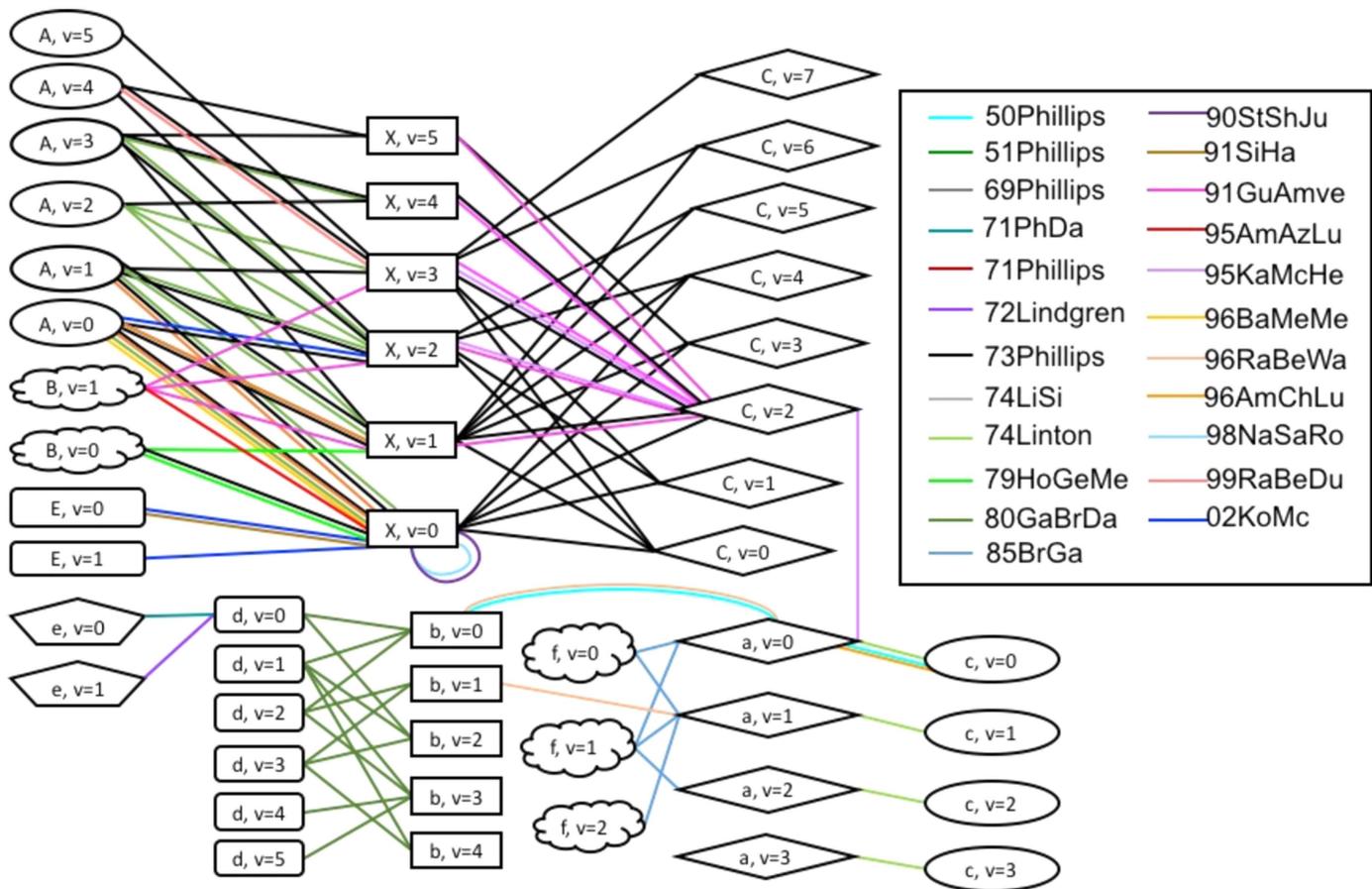
Figure 2. Vibronic structure of the $^{48}Ti^{16}O$ spectroscopic network.

along the internuclear axis, described by the Ω quantum number, is equal to Λ, as for singlet states $\Sigma = 0$.

For some states, the parity affects the final energy significantly enough to be experimentally observable; usually these states are of Π symmetry. In these cases, we will append the parity to the electronic state label. The parity of the energy level can be specified as (e/f) (Brown et al. 1975). For electronic dipole allowed transitions, the selection rules are $e \leftrightarrow e$ and $f \leftrightarrow f$ for P and R branches ($\Delta J = \pm 1$) and $e \leftrightarrow f$ for Q branches ($\Delta J = 0$). For Π states with experimental evidence of the splitting of the states, we distinguish between the e and f parity states. For the B $^3\Pi$ and E $^3\Pi$ states, the two parity states cannot be unambiguously assigned as e and f; therefore, following the recommendations of Brown et al. (1975), we retain the a and b designations (Mulliken 1955) employed in the original manuscripts. For the b $^1\Pi$ state, the b $^1\Pi$–d $^1\Sigma^+$ transitions occur from the d $^1\Sigma^+$ state of well-defined parity e, which fixes the parity of the observed levels of the associated b $^1\Pi$ state.

2.4. Collation of Data Sources

The collated data sources used in the rotationally resolved MARVEL analysis are summarized in Table 1. In total, we use 24 data sources, involving 11 electronic states with 49,679 transitions, 123 total (non-unique) vibronic bands, and 84 total unique vibronic bands. The full list of compiled data converted to MARVEL format is in the supplementary information; an extract is given in Table 2.

There are a number of data sources, particularly from the early–mid-twentieth century, which provide data on positions of bands (usually band-heads, though sometimes this is unspecified). Often these early studies went to significantly higher vibrational levels than more modern experiments, which have tended to focus on very high accuracy rotationally resolved lines. These two types of data are often quite complementary and together build a rather extensive understanding of the rovibronic energies of the molecule. We have collated data sources with information on bands in Table 3.

Another important type of data are measurements of the intensity of bands and the lifetimes of states. The sources of these data have been collated in Table 4. These data are not used here but will be used later to verify the dipole moment curves for the Duo spectroscopic model of TiO.

There are a number of other studies of TiO spectra that we have not been used in this study for various reasons. These data sources are collated in Table 5 with comments.

2.5. Comments on the Rotationally Resolved Data Sources (Table 1)

Many papers give uncertainties that we adopt unaltered and found to be reasonably consistent with all other TiO data (i.e., a relatively small number of transitions needed adjusted uncertainties or could not be verified), specifically: $0.02\,cm^{-1}$ (for unblended lines, up to $0.07\,cm^{-1}$ for unblended lines) in 74Linton, $0.008\,cm^{-1}$ (unblended lines) for 79HoGeMe, $0.01\,cm^{-1}$ in 80GaBrDa, $0.044\,cm^{-1}$ in 85BrGa, $0.03\,cm^{-1}$
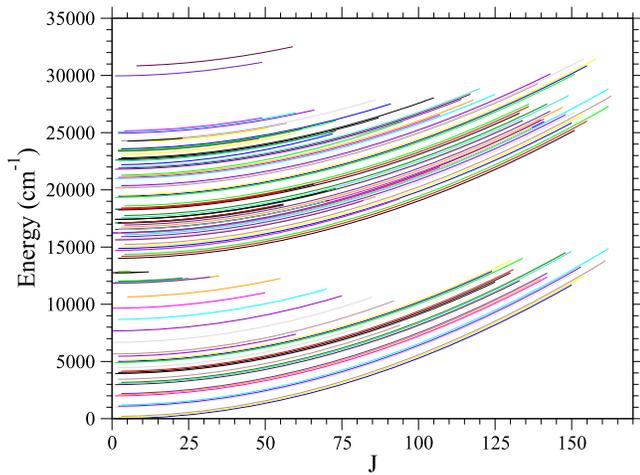
Figure 3. Summary of characterized energy levels. Different lines indicate different spin-vibronic states.

Table 6
Extract from the 48Ti-16O.energies Output File for $^{48}Ti^{16}O$

State	J	v	$\tilde{E}$	Unc.	No
X3Delta_1	1	0	0.0	0.00001	36
X3Delta_1	2	0	2.111897	0.000007	50
X3Delta_1	3	0	5.279694	0.00001	60
X3Delta_1	4	0	9.505353	0.000199	59
X3Delta_1	5	0	14.78605	0.000199	58
X3Delta_1	6	0	21.121889	0.000001	65
X3Delta_1	7	0	28.513037	0.000001	61
X3Delta_1	8	0	36.959873	0.000001	68
X3Delta_1	9	0	46.463111	0.000001	70
b1Pi	86f	0	18511.91059	0.008909	3
A3Phi_3	43	4	18513.79788	0.003993	10
A3Phi_2	47	4	18514.59668	0.003993	10
A3Phi_3	14	5	18514.86149	0.11547	3
b1Pi	20e	4	18518.44328	0.005774	3
A3Phi_3	83	1	18520.93357	0.005725	18
A3Phi_4	39	4	18522.97952	0.003672	10
A3Phi_3	15	5	18529.54712	0.11547	3
A3Phi_2	24	5	18532.63495	0.11547	3
B3Pi_0	68b	0	18535.06106	0.11547	3
B3Pi_1	67b	0	18535.90423	0.11547	3
B3Pi_0	68a	0	18536.51772	0.11547	3
B3Pi_1	67a	0	18536.5709	0.11547	3
B3Pi_2	66a	0	18538.92466	0.141421	2
B3Pi_2	66b	0	18538.92466	0.141421	2
b1Pi	21e	4	18539.41806	0.005774	3
b1Pi	21f	4	18539.49211	0.01	1
A3Phi_2	75	2	18540.01583	0.057735	12
B3Pi_0	54b	1	18540.12798	0.008	1

Note. Energies and uncertainties are given in cm^{-1}. "No" indicates the number of transitions that contributed to the stated energy and uncertainty.

(This table is available in its entirety in machine-readable form.)

in 91GuAmVe, $0.1\,cm^{-1}$ in 91SiHaxx, $0.01\,cm^{-1}$ in 95KaMcHe, $0.002\,cm^{-1}$ in 96BaMeMe, and $0.02\,cm^{-1}$ in 96RaBeWa. Other comments related to Table 1 are as follows.

(1a) Data due to Phillips (50Phillips, 51Phillips, 69Phillips, 71PhDa, 71Phillips, 73Phillips-AX, 73Phillips-BX, and 73Phillips-CX) are obtained from photographic plates. Originally, we used $0.045\,cm^{-1}$ as the estimated

Table 7
Summary of Energy Levels Found Through the MARVEL Analysis

	v	p	J Range	Uncertainties (cm^{-1})		
				Min	Aver.	Max
X $^3\Delta_1$	0		1–150	0.0002	0.021	0.12
	1		1–150	0.0013	0.026	0.14
	2		1–142	0.0016	0.034	0.2
	3		1–133	0.0016	0.039	0.2
	4		1–125	0.0028	0.068	0.2
	5		1–134	0.02	0.086	0.2
X $^3\Delta_2$	0		2–154	0.0002	0.022	0.1
	1		2–153	0.0012	0.025	0.2
	2		2–140	0.0016	0.029	0.2
	3		2–150	0.0016	0.04	0.2
	4		2–130	0.0028	0.062	0.2
	5		2–124	0.028	0.1	0.2
X $^3\Delta_3$	0		3–161	0.00048	0.029	0.14
	1		3–162	0.0013	0.036	0.14
	2		3–142	0.0018	0.036	0.2
	3		3–148	0.0017	0.055	0.26
	4		3–131	0.0035	0.097	0.2
	5		3–130	0.02	0.086	0.2
A $^3\Phi_2$	0		2–151	0.0002	0.031	0.2
	1		2–150	0.0015	0.031	0.14
	2		2–151	0.0016	0.048	0.2
	3		2–141	0.0018	0.05	0.2
	4		2–134	0.0023	0.047	0.14
	5		2–133	0.12	0.13	0.2
A $^3\Phi_3$	0		3–155	0.0002	0.029	0.2
	1		3–154	0.0013	0.029	0.2
	2		3–148	0.0016	0.038	0.2
	3		3–147	0.0018	0.053	0.2
	4		3–149	0.0023	0.071	0.42
	5		3–136	0.12	0.13	0.2
A $^3\Phi_4$	0		4–162	0.00048	0.041	0.14
	1		4–163	0.0014	0.045	0.2
	2		4–162	0.0017	0.061	0.2
	3		4–143	0.0023	0.07	0.2
	4		4–142	0.0023	0.063	0.2
	5		4–136	0.12	0.13	0.2
B $^3\Pi_0$	0	a	0–141	0.0033	0.084	0.2
	0	b	1–137	0.004	0.075	0.2
	1	a	2–56	0.0033	0.0046	0.0081
	1	b	1–55	0.0035	0.0058	0.014
B $^3\Pi_1$	0	a	0–102	0.0032	0.046	0.2
	0	b	0–107	0.0039	0.063	0.18
	1	a	1–53	0.0023	0.0051	0.03
	1	b	2–55	0.0036	0.0072	0.03
B $^3\Pi_2$	0	a	2–140	0.0035	0.081	0.2
	0	b	3–140	0.004	0.082	0.2
	1	a	2–56	0.0033	0.0058	0.017
	1	b	3–54	0.004	0.006	0.0094
C $^3\Delta_1$	0		1–151	0.071	0.082	0.14
	1		1–139	0.082	0.092	0.2
	2		1–125	0.017	0.092	0.2
	3		1–114	0.082	0.11	0.36
	4		1–73	0.082	0.088	0.2
	5		2–48	0.1	0.11	0.2

Table 7
(Continued)

	v	p	J Range	Uncertainties (cm^{-1})		
				Min	Aver.	Max
	6		13–51	0.1	0.11	0.2
	7		2–66	0.14	0.16	0.2
C $^3\Delta_2$	0		2–155	0.071	0.09	0.2
	1		2–154	0.082	0.1	0.2
	2		2–107	0.028	0.082	0.2
	3		2–117	0.082	0.094	0.2
	4		2–87	0.082	0.089	0.2
	5		2–73	0.1	0.12	0.36
	6		3–57	0.1	0.11	0.2
	7		2–60	0.14	0.15	0.2
C $^3\Delta_3$	0		3–158	0.071	0.089	0.2
	1		3–143	0.082	0.097	0.2
	2		3–118	0.0036	0.067	0.2
	3		3–120	0.082	0.1	0.2
	4		3–105	0.082	0.094	0.2
	5		3–91	0.1	0.11	0.33
	6		3–86	0.1	0.12	0.23
	7		4–49	0.14	0.15	0.2
E $^3\Pi_0$	0	a	0–35	0.0057	0.0069	0.01
	0	b	0–32	0.0057	0.0068	0.01
	1	a	1–13	0.0058	0.0085	0.01
	1	b	0–12	0.0058	0.0076	0.011
E $^3\Pi_1$	0	a	1–25	0.0058	0.0066	0.01
	0	b	1–25	0.0058	0.0067	0.01
	1	a	2–6	0.01	0.01	0.01
	1	b	2–6	0.01	0.01	0.01
E $^3\Pi_2$	0	a	2–23	0.0058	0.0065	0.0071
a $^1\Delta$	0		2–100	0.0024	0.0073	0.14
	1		2–92	0.0063	0.034	0.32
	2		2–60	0.011	0.013	0.022
	3		5–59	0.011	0.014	0.021
b $^1\Pi$	0	e	1–99	0.0038	0.0077	0.1
	0	f	1–99	0.0051	0.0086	0.028
	1	e	1–86	0.0034	0.0079	0.058
	1	f	1–82	0.0046	0.0063	0.013
	2	e	1–71	0.0041	0.0069	0.023
	2	f	2–70	0.0058	0.0077	0.035
	3	e	1–73	0.0045	0.0087	0.029
	3	f	1–70	0.0058	0.01	0.056
	4	e	1–66	0.0058	0.011	0.066
	4	f	3–56	0.0071	0.0096	0.019
c $^1\Phi$	0		3–101	0.0028	0.016	0.2
	1		3–93	0.011	0.052	0.49
	2		3–60	0.011	0.013	0.02
	3		6–59	0.011	0.014	0.021
d $^1\Sigma^+$	0		0–92	0.0033	0.0045	0.01
	1		0–85	0.0029	0.0047	0.028
	2		0–75	0.0033	0.0054	0.01
	3		2–70	0.0038	0.0065	0.02
	4		0–50	0.0058	0.0088	0.024
	5		2–55	0.0071	0.0094	0.01
e $^1\Sigma^+$	0		1–49	0.035	0.041	0.053
	1		8–59	0.035	0.04	0.078

Table 7
(Continued)

	v	p	J Range	Uncertainties (cm^{-1})		
				Min	Aver.	Max
f $^1\Delta$	0		2–71	0.019	0.023	0.044
	1		2–62	0.018	0.023	0.044
	2		5–23	0.031	0.039	0.044

uncertainty for these data. However, we found significant inconsistencies with this uncertainty and increased it to 0.1 cm^{-1} for data published in these papers and 0.2 cm^{-1} for data found from external sources (though these data have been analyzed within the published papers).

(1b) 51Phillips incorrectly assigns that the γ band to the a $^3\Delta$–$^3\Pi$ band; it is actually a $^3\Phi$–$^3\Delta$ band (the lowest state at that stage was believed to be X $^3\Pi$). We have modified the *state* and Ω quantum numbers.

(1c) 69Phillips incorrectly identifies the band as the unphysical B $^3\Pi_1$–X $^3\Delta_0$ in the data table only, rather than B $^3\Pi_0$–X $^3\Delta_1$ (as in the text).

(1d) 50Phillips-ext and 73Phillips data were obtained from tapes given by Phillips to Kurucz in 1981 (these data are not in the original publication). It is not clear if the c-a data from this tape data has been published; we have chosen to link the data to the original Phillips c-a paper, i.e., 50Phillips-ext. The bandhead details from the A-X, B-X, and C-X data are given in 73Phillips; thus we assign the tape data on these bands to this paper. The tape data has 174 transitions, which have unphysical assignments, $J \leqslant |\Omega - \Sigma|$; e.g., an A $^3\Phi$ energy level with J < 2. There are 55 C-X, 112 A-X and 7 c-a unphysical transitions. There is some repetition between data in the 73Phillips compilation and earlier data, e.g., the 71Phillips B-X data. However, the tape compilation of data is significantly more extensive while the former has been published explicitly assigned. Therefore, we use both. Note that the number of unverified transitions from these data is significantly higher than other data sources; however, as the resulting energies were reasonable, we chose not to exclude these data sets. We note that these data have been used to inform some of the available TiO line lists, particularly the recent update of the Plez (1998) line list for inclusion in the VALD database (Ryabchikova et al. 2015).

(1e) 72Linton: obs-calc was given as 0.03 cm^{-1}; however, we found that uncertainties of 0.05 cm^{-1} were more consistent with other measurements.

(1f) 72Lindgren gives no uncertainties; we used 0.05 cm^{-1} (based on 72Linton), which gave self-consistent results.

(1g) 79HoGeMe: a full set of data was obtained from C. Amiot (2015, private communication). Only the 0-0 data were provided in the original paper.

(1h) 79GaDe provides rovibrational energy levels, but does not distinguish between the spectra of different spin components; we have used the median $S = 0$, i.e., $\Omega = 2$ for the associated energy levels.

(1i) 90StShJu: the stated uncertainty is 0.5 MHz, on the order of 10^{-5} cm^{-1}, which has been adopted.

(1j) 91GuAmVe data were obtained from C. Amiot (2015, private communication).

Table 8
Triplet Vibronic Level Origins from MARVEL Data, and Difference from Schwenke (1998) Line List Data, ^{48}Ti^{16}O; $J_{min} = \Omega$ unless Otherwise Specified; All Numbers Are Given in cm^{-1}

v	X $^3\Delta_1$		X $^3\Delta_2$		X $^3\Delta_3$	
0	0.0000(2)	+0.0000	98.9039(2)	−0.036	203.7006(5)	−0.0229
1	1000.019(5)	+0.003	1098.922(6)	−0.030	1203.711(6)	−0.015
2	1990.89(9)	−0.01	2089.790(4)	−0.036	2194.579(5)	−0.026
3	2972.55(9)	+0.02	3071.45(9)	−0.013	3176.235(7)	−0.004
4	3945.2(1)	−0.2	4044.1(1)	−0.181	4148.70(1)	+0.01
5	4908.3(1)	+0.0	5007.3(1)	−0.123	5112.0(1)	−0.0

v	A $^3\Phi_2$		A $^3\Phi_3$		A $^3\Phi_4$	
0	14021.6986(2)	+0.0369	14197.6325(2)	+0.0302	14370.4654(5)	−0.0572
1	14881.69(6)	−0.11	15057.388(3)	+0.026	15229.94(7)	+0.04
2	15734.01(6)	+0.09	15909.39(6)	−0.00	16081.55(6)	+0.06
3	16578.51(6)	+0.04	16753.58(6)	−0.06	16925.45(6)	+0.02
4	17414.91(7)	−0.19	17589.85(7)	−0.12	17761.44(7)	−0.02
5	18243.4(2)	+0.3	18418.0(1)	−0.0	18589.4(1)	−0.0

v	B $^3\Pi_0$		B $^3\Pi_1$		B $^3\Pi_2$	
0	16225.767(6)	1	16248.457(6)	2	16267.360(6)	
1	17089.313(8)$^{J=1}$	1	17112.64(3)	2	17131.681(8)	

v	C $^3\Delta_1$		C $^3\Delta_2$		C $^3\Delta_3$	
0	19341.5(1)	−0.7	19442.3(1)	+1.0	19537.2(1)	+0.9
1	20170.1(1)	−0.3	20271.3(1)	+0.9	20365.5(1)	+0.8
2	20990.6(1)	−0.8	21091.4(1)	+0.8	21181.262(4)	−0.051
3	21802.4(2)	−1.7	21902.8(1)	+0.3	21993.3(1)	+0.1
4	22605.3(1)	−3.0	22704.6(1)	−0.2	22797.0(1)	+0.1
5	23401.9(2)$^{J=2}$		23497.1(2)	−0.2	23591.9(2)	−0.3
6	24252.0(1)$^{J=13}$		24283.2(2)$^{J=3}$	3	24376.7(2)	
7	24952.4(2)$^{J=2}$		25053.7(2)	4	25155.5(2)$^{J=4}$	

v	E $^3\Pi_0$		E $^3\Pi_1$		E $^3\Pi_2$	
0	11838.204(5)	1	11924.082(5)	2	12013.724(5)	
1	12752.166(4)	2	12838.667(5)			

(1k) 96AmChLu state that the width of the lines under their experimental conditions was 0.005 cm^{-1}; we adopted this as the estimated uncertainty of the line position.

(1l) 98NaSaRo estimated uncertainty is 8 kHz, equivalent to 10^{-7} cm^{-1}, which has been adopted.

(1m) 99RaBeDu laboratory and sunspot (SS) measurements: the need for consistency with other measurements (and to maximize the number of validated transitions and minimize the need for increased uncertainties of some lines) meant that we doubled the uncertainties from the original paper from 0.02 and 0.005 cm^{-1} for lab and sunspot data to 0.004 and 0.01 cm^{-1}.

(1n) 02KoHaMc uncertainties estimates were given as 0.002–0.005 cm^{-1}; however, 0.01 cm^{-1} seems to be a more reasonable estimate based on the overall MARVEL model. This value was adopted.

2.6. Comments on Data Sources for Band-head Information (Table 3)

(3a) 69LiNi suggests assignments for two bands in the 28Lowater data, 7 in the 37WuMe data, and 1 in the 57GaRoJu data.

(3b) 29Christya has rotationally resolved data, but more recent higher resolution data sources are available, so we only used the band-head information.

(3c) 72PhDa and 77LiBrb: it is assumed that the wavelengths are taken in air at standard temperature and pressure; a refraction index of 1.00029 is used to convert to frequency in vacuum.

3. MARVEL Energy Levels

3.1. Spectroscopic Networks

The vibronic structure of the spectroscopic network of the experimentally assigned TiO transitions is shown in Figure 2. Probably the most important observed transitions are the spin-forbidden C $^3\Delta$–a $^1\Delta$ transitions from Kaledin et al. (1995) that allow the relative energy of the triplet and singlet manifolds to be fixed. The figure makes clear that the X $^3\Delta$, A $^3\Phi$, and C $^3\Delta$ states, up to high vibrational energies, are well characterized. There are a number of sources providing vibrational connections, though further observations of the vibrationally excited C $^3\Delta$–X $^3\Delta$ transitions with modern techniques would be beneficial.

No transitions involving the B $^3\Pi$ state higher than $v = 1$ have been assigned in rotationally resolved spectra. The bond lengths of the A $^3\Phi$ and B $^3\Pi$ states are comparable and

Table 9
Singlet Vibronic Level Origins in cm^{-1} for ^{48}Ti^{16}O; $J_{min} = \Lambda$ (=Ω) Unless Otherwise Specified

	v	J	MARVEL	Schwenke (1998)
a $^1\Delta$	0	2	3446.481(8)	−0.044
	1	2	4455.67(2)	−0.03
	2	2	5455.83(2)	+0.022
b $^1\Pi$	0	1	14717.055(9)	+3.016
	1	1	15628.21(1)	+3.175
	2	1	16530.741(6)	+3.176
	3	1	17424.48(1)	+3.14
	4	1	18309.459(7)	+2.995
c $^1\Phi$	0	3	21290.11(1)	+0.20
	1	3	22199.59(2)	−0.145
	2	3	23099.06(1)	−0.127
d $^1\Sigma^+$	0	0	5661.92(1)	+0.03
	1	0	6675.304(7)	−0.08
	2	0	7678.78(1)	−0.04
	3	2	8675.824(7)	−0.080
	4	0	9656.64(1)	−0.07
	5	5	10646.90(1)	−0.07
e $^1\Sigma^+$	0	1	29960.98(5)	
	1	8	30839.17(5)	
f $^1\Delta$	0	2	22515.29(3)	
	1	2	23384.44(4)	
	2	5	24260.42(3)	

significantly larger than the bond length of the X $^3\Delta$ state; we thus expect that B $^3\Pi$–X $^3\Delta$ Franck–Condon transitions with higher changes in vibrational quantum number should be observable like the A $^3\Phi$–X $^3\Delta$ transitions. Indeed, as discussed below, band-heads for these transitions have been assigned.

The E $^3\Pi$ state is sparsely characterized and the key experiments by Kobayashi et al. (2002) were only performed after construction of the seminal TiO line lists of Jorgensen (1994), Plez (1998), and Schwenke (1998). In particular, the observation of the $v = 1$ band allow a reasonable Morse oscillator fit to the E $^3\Pi$ state potential energy curve that previously only was characterized by its ground vibrational level.

Taken together, the experimental observations of the singlet states produce an almost completely connected network. For example, none of the c $^1\Phi$–a $^1\Delta$ transitions from Linton (1974) involve a change in the vibrational quantum number due to the near parallel curves for the two states; by themselves these give no absolute vibrational energies. However, the f $^1\Delta$–a $^1\Delta$ transitions do often involve changes in the vibrational quantum number and allow the absolute vibrational energies of the c $^1\Phi$ and a $^1\Delta$ states to be extracted. These sorts of arguments are common in the singlet manifold; due to this, there is only one band unconnected to the large TiO spectroscopic network: the transitions between the c $^1\Phi$ ($v = 3$) and a $^1\Delta$ ($v = 3$) states. This band is treated as a floating component in this study. Unlike in the triplet manifold, however, most transitions in the singlet manifold have only been measured once and often this is pre-1990s. Modern re-measurements would allow higher accuracy results for the singlet energy levels of TiO.

3.2. MARVEL Energy Levels

The final energy levels from the MARVEL analysis are collated in the supplementary information. An extract from this file, together with a description of each column, is provided in Table 6. The data of Table 6 for the X $^3\Delta_1$, X $^3\Delta_2$, and X $^3\Delta_3$ states, where the subscript corresponds to the three possible Ω values, confirm that the three fine-structure states have very slightly different "rotational" levels and that transitions have been observed within all three fine-structure states. Note also that only a very small number of transitions within a fine-structure state have been measured, which calls for further experimental studies.

Figure 3 shows graphically the energy against the total angular momentum for all different spin-vibronic states in the main spectroscopic network. The triplets can be identified by near parallel closely spaced lines. The vibrational levels of each electronic state are separated by approximately 1000 cm^{-1}. The fact that all curves are smooth quadratics provides confidence in the extracted MARVEL energy levels.

Table 7 tabulates the number of MARVEL energy levels that have been obtained for each spin-vibronic state, including the minimum, average, and maximum uncertainty of the levels and the J range covered. In the X $^3\Delta$, A $^3\Phi$, and C $^3\Delta$ states, quite high vibrational excitations have been observed, which should facilitate high accuracy in the spectroscopically refined potential energy curves (PEC) for these states. However, in the E $^3\Pi$ and B $^3\Pi$ states, only the ground and first excited vibrational states have available data. The a $^1\Delta$, b $^1\Pi$, c $^1\Phi$, and d $^1\Sigma^+$ singlet states have been well characterized to moderate vibrational excitations, which will permit good refinement of the PECs. The e $^1\Sigma^+$ and f $^1\Delta$ states have two and three vibrational levels characterized, respectively; this will permit reasonable first-order approximations to the PECs. Note, however, that the number of perturbing states at higher excitation energies is very large and the potential energy curves of the more highly excited states (particularly the e $^1\Sigma^+$ state) are likely to be strongly affected.

4. Discussion

4.1. Vibronic Band Origins

The triplet and singlet vibronic level origins from the MARVEL data are given in Tables 8 and 9, respectively. In most cases, the level given is the lowest possible J for that spin-vibronic state; however, there are some cases (e.g., high vibrational states of the C $^3\Delta$ state) where this level was not observed. These MARVEL data will soon be used with high-level ab initio data to construct a full spectroscopic model of ^{48}Ti^{16}O; this can be used to predict the lowest J energy levels for all states, as well as higher vibrational levels not accessed by rotationally resolved ^{48}Ti^{16}O data.

The C $^3\Delta_3$($v = 2$) origin and the c $^1\Phi$ ($v = 0$) origin are separated by about 120 cm^{-1} and are spin–orbit coupled; the resulting perturbations have been extensively studied, see Namiki et al. (2003a). The vibronic band origins are consistent with the spectroscopic parameters (term energies, vibrational frequencies, and spin–orbit couplings) extracted previously from individual experiments using model Hamiltonians.

Table 10
Triplet A $^3\Phi$ − X $^3\Delta$ R-branch Band-heads in cm^{-1} for ^{48}Ti^{16}O

v'–v''	A $^3\Phi_2$ − X $^3\Delta_1$ (c)			A $^3\Phi_3$ − X $^3\Delta_2$ (b)			A $^3\Phi_4$ − X $^3\Delta_3$ (a)		
	J	MARVEL	Low-res obs.	J	MARVEL	Low-res obs.	J	MARVEL	Low-res obs.
0–0	20	14030.258	14030.1 [1]	18	14105.342	14104.7 [1]	17	14171.984	14171.4 [1]
0–1	23	13031.547		20	13106.365		19	13172.872	
0–2	26	12042.400		23	12116.854		21	12183.165	
0–3[a]	31	11063.037		26	11136.944		24	11203.004	
0–4[a]	37	10093.892		31	10166.938		28	10232.599	
0–5[a]	46	9135.714		38	9207.438		34	9272.352	
1–0	18	14889.145	14889.4 [1]	16	14964.137	14963.6 [1]	15	15030.610	15030.1 [1]
1–1	20	13890.137	13889.6 [1]	18	13964.949	13964.5 [1]	17	14031.319	14030.1 [1]
1–2	23	12900.552		20	12975.114		19	13041.355	
1–3	26	11920.557		23	11994.751		21	12060.818	
1–4[a]	30	10950.355		26	11024.037		24	11089.856	
1–5[a]	37	9990.374		32	10063.272		28	10128.667	
2–0	16	15740.491	15743.1 [1]	15	15815.347	15814.7 [1]	14	15881.637	
2–1	18	14741.273	14741.3 [1]	16	14815.991		15	14882.195	
2–2	20	13751.408		18	13825.938		17	13892.056	
2–3	22	12770.968		20	12845.272		18	12911.259	
2–4	26	11800.133		23	11874.095		21	11939.912	
2–5[a]	30	10839.158		25	10912.584		24	10978.171	
3–0[a]	15	16584.161		14	16658.838		12	16724.832	
3–1	16	15584.788	15586.3 [1]	15	15659.365	15658.9 [1]	14	15725.306	
3–2	18	14594.705	14594.0 [1]	16	14669.158	14669.1 [1]	15	14735.027	
3–3[a]	19	13613.992		18	13688.271		16	13754.043	
3–4	22	12642.744		20	12716.789		18	12782.465	
3–5	26	11681.134		23	11754.775		21	11820.357	
4–0[a]	13	17420.027		12	17494.548		12	17560.413	
4–1[a]	14	16420.538		13	16494.964		13	16560.785	
4–2	16	15430.316	15430.2 [1]	15	15504.628	15505.4 [1]	14	15570.404	
4–3	17	14449.410		16	14523.591	14522.8 [1]	15	14589.288	14588.0 [1]
4–4[a]	19	13477.864		17	13551.898		16	13617.525	
4–5	22	12515.842		20	12589.596		18	12655.156	
5–0[a]	12	18248.069		11	18322.338		10	18387.978	
5–1[a]	13	17248.458		12	17322.646		12	17388.282	
5–2[a]	15	16258.090	16258.9 [1]	13	16332.224		12	16397.805	
5–3	15	15277.035	15276.6 [1]	14	15351.024	15350.6 [1]	14	15416.585	
5–4[a]	17	14305.324		16	14379.181		15	14444.694	
5–5[a]	19	13343.000		19	13416.662		16	13482.091	

Note. [1] 28Lowater (Lowater 1928).
[a] MARVEL predicted band-heads.

4.2. Prediction of Unmeasured Lines

The MARVEL spin-rovibronic states for which we have assigned energies will be involved in more transitions than were used in their generation. The tabulation and analysis of these potential transitions provides key information, which can be used to assist assignment of new spectra. We have produced a list of all transitions between MARVEL energy levels that obey the following selection rules: $|\Delta J| \leqslant 1$, $|\Delta\Lambda| \leqslant 1$ and $\Delta S = 0$. This data is provided in the supplementary information.

4.3. Band-heads

Tables 10–14 tabulate the MARVEL-derived band-heads for each spin–vibronic state and compare these band-heads against low-resolution observations of band-heads from the references tabulated in Table 3. Additionally, there are some band-heads that have been experimentally observed and assigned and involve some spin–vibronic states not studied in any high-resolution study that are thus not in the MARVEL analysis.

These will be very useful to verify the final DUO spectroscopic model for ^{48}Ti^{16}O in a future study. Furthermore, we tabulate the approximate J for the band-head based on the transition frequencies derived from MARVEL energy levels; this can be used to help suggest a J value associated with these other experimentally observed band-heads.

Table 10 provides the A $^3\Phi$–X $^3\Delta$ R-band-heads. Agreement between the low-resolution and MARVEL band-heads is generally within 2 cm^{-1}.

Table 11 gives the B $^3\Pi$–X $^3\Delta$ R-band-heads: five have been observed in rotationally resolved spectra, six have positions predicted by MARVEL data, and nine other band-heads have been observed in low-resolution non-rotationally resolved observations. Of the 28 low-resolution band-heads observed by 69Phillips, 9 were also calculated using MARVEL data. Most agree with our calculations to around a few cm^{-1}, but there are clearly some mis-assignments for the 15,930 and 16,081 cm^{-1} band-heads. The higher vibrational levels of the B $^3\Pi$ state have yet to be observed in a rotationally resolved study, but

Table 11
Triplet B $^3\Pi$ − X $^3\Delta$ R-branch Band-heads in cm^{-1} for ^{48}Ti^{16}O

v'–v''	B $^3\Pi_0$ − X $^3\Delta_1$			B $^3\Pi_1$ − X $^3\Delta_2$			B $^3\Pi_2$ − X $^3\Delta_3$		
	J	MARVEL	Low-res obs.	J	MARVEL	Low-res obs.	J	MARVEL	Low-res obs.
0–0	12	16233.187	16233 [1]	17	16160.243	16160 [2]	28	16085.853	16085 [2]
			16233 [2]			16160 [2]			16085 [2]
0–1	13	15233.618	15218 [1]	19	15161.155	15156 [2]	32	15088.458	15081 [1]
0–2[a]	15	14243.289		22	14171.535		36	14101.011	
0–3[a]	16	13262.269		26	13191.512		41	13123.750	
0–4[a]	18	12290.645		31	12221.408		47	12157.203	
0–5[a]	22	11328.578		38	11261.867		57	11202.350	
1–0	12	17096.309	17098 [1]	15	17023.495	17022 [2]	25	16947.583	16950 [1]
			17095 [2]			17022 [2]			16950 [2]
1–1	12	16096.673	16081 [1]	17	16024.203	16022 [1]	28	15949.664	15930 [1]
			16096 [2]			16023 [2]			15949 [2]
1–2	14	15106.267		19	15034.244		31	14961.413	
1–3	15	14125.142		22	14053.757		35	13983.062	
1–4[a]	17	13153.331		25	13082.904		41	13014.997	
1–5[a]	19	12190.954		30	12121.999		48	12057.532	
2–0[a]			17952 [1]			17881 [1]			17804 [1]
2–1[a]			16931 [1]			16877 [1]			16799 [1]
						16881 [2]			16804 [2]
2–2[a]			15961 [2]			15887 [1]			15814 [2]
						15887 [2]			
3–0[a]						18727 [1]			
3–1[a]			17804 [1]			17722 [1]			17650 [1]
3–2[a]			16799 [1]			16717 [1]			16654 [1]
						16736 [2]			16663 [2]
4–2[a]			17650 [1]			17579 [1]			17502
4–3[a]			16654 [1]			16574 [1]			16504 [1]
						16596 [2]			16521 [2]
5–4[a]						16332 [2]			16382 [2]

Note. [1] 69Phillips (Phillips 1969), [2] 76ZyPa (Zyrnicki & Palmer 1976)
[a] MARVEL predicted band-heads.

there is significant band-head information that can be very valuable in fitting the B $^3\Pi$ state PEC for the final spectrosopic model of ^{48}Ti^{16}O. Further high-resolution rotationally resolved studies would be welcome.

Table 12 tabulates C $^3\Delta$–X $^3\Delta$ R-band-heads. There is very extensive coverage both rotationally resolved and low-resolution band-head observations. There is good agreement (within a couple of cm^{-1}) between almost all MARVEL and low-resolution observations. Band-heads from transitions with large Δv can be predicted from MARVEL data despite not being directly observed due to either congestion in the spectra and/or low intensity due to small Franck–Condon factors.

Table 13 tabulates E $^3\Pi$–X $^3\Delta$ R-band-heads. The coverage of high vibrational levels of the E $^3\Pi$ state in the low-resolution observed band-heads is much more extensive than any rotationally resolved data and will be valuable for the future DUO model. Again, high-resolution studies of these bands would be valuable.

For the singlet states (band-heads shown in Table 14), the rotationally resolved data in combination with the MARVEL predicted band-heads are generally more extensive and accurate than the low-resolution observations. The key exception is probably the c $^1\Phi$–a $^1\Delta$ data, for which low-resolution data exist involving vibrational levels up to $v = 4$, including transitions with ($\Delta v \neq 0$). The agreement between the MARVEL

energies and the low-resolution observations is generally high, except for the f $^1\Delta$–a $^1\Delta$ data. The band-head assignments from DeVore (1982) involving higher vibrational quantum numbers do not agree with the MARVEL data obtained mostly from the rotationally resolved study of Brandes & Galehouse (1985). The difference between these two assignments is in the vibrational frequency of the f $^1\Delta$ level; it is likely that the higher resolution rotationally resolved data we have used are the correct assignment.

4.4. Comparison with Schwenke (1998)

Figure 4 compares the MARVEL energy levels against those derived by Schwenke (1998) for the triplet states. The X $^3\Delta$ and A $^3\Phi$ states have differences of generally less than 0.01 cm^{-1} for J < 50, with larger errors for higher rotational levels. The E $^3\Pi$ state has significant errors up to 2 cm^{-1}; this is partially to be expected as a significant source of experimental data for this state post-dates Schwenke's work. Many of the B $^3\Pi$ state levels have quite high errors around 3 cm^{-1}. Most of the B $^3\Pi$ state data come from Hocking et al. (1979), so for the most part Schwenke should have used the same data as us. The error bars on these data are much smaller than differences in the energy levels. Schwenke reports some difficulty in the fitting, giving an RMSE of 0.743 cm^{-1} for these lines. For the C $^3\Delta$ state, there are significant differences between Schwenke's

Table 12
C $^3\Delta$ − X $^3\Delta$ R-branch Band-heads for ^{48}Ti^{16}O

$v'-v''$	C $^3\Delta_1$ − X $^3\Delta_1$			C $^3\Delta_2$ − X $^3\Delta_2$			C $^3\Delta_3$ − X $^3\Delta_3$			C $^3\Delta$ − X $^3\Delta$
	J	MARVEL	Low-res obs.	J	MARVEL	Low-res obs.	J	MARVEL	Low-res obs.	Low-res obs.
0–0	11	19347.333	19347 [2]	11	19349.241	19349 [2]	11	19339.917	19340 [2]	19348 [3]
0–1	12	18347.688	18347 [2]	12	18349.571	18349 [2]	12	18340.234	18339 [2]	18350 [3]
0–2	13	17357.230	17358 [1]	13	17359.1176	17361 [1]	13	17349.818	17350 [1]	17359 [3]
0–3	14	16376.034		13	16377.898		14	16368.658		16378 [3]
0–4[a]	15	15404.171		15	15405.969		15	15396.793		
0–5[a]	17	14441.577		16	14443.352		17	14434.300		
1–0	10	20175.638	20177 [2]	10	20177.880	20178 [2]	10	20167.862	20168 [2]	20176 [3]
1–1[a]	11	19175.912		11	19178.139		12	19168.148		
1–2	12	18185.422		12	18187.640		12	18177.671		18186 [2]
										18186 [3]
1–3	13	17204.151	17204 [1]	13	17206.354	17207 [2,3]	13	17196.403	17192 [1]	
1–4[a]	14	16232.174	16231 [1]	14	16234.350		14	16224.432		
			16232 [2]							
1–5[a]	15	15269.512		15	15271.589		16	15261.827	15264 [1]	
2–0	10	20995.714	20995 [2]	9	20997.734	20997 [2]	10	20983.435	20983 [2]	20998 [3]
2–1	10	19995.958	19995 [2]	9	19997.910	19996 [2]	11	19983.702	19984 [2]	19998 [3]
2–2	10	19005.366		11	19007.348		12	18993.166		
2–3	12	18024.053		11	18025.981		13	18011.876		18026 [3]
2–4	13	17051.956	17051 [1]	12	17053.891	17055 [2]	13	17039.866		17054 [3]
2–5	13	16089.177		14	16091.005		15	16077.182		16086 [2]
3–0	9	21807.075	21806 [2]	9	21808.677	21809 [2]	10	21795.164	21795 [2]	21809 [3]
3–1	9	20807.262	20807 [2]	9	20808.853	20810 [2]	10	20795.391	20796 [2]	20810 [3]
3–2[a]	11	19816.669		11	19818.257		10	19804.784		
3–3[a]	11	18835.356		11	18836.890		11	18823.417		18835 [2]
3–4[a]	11	17863.148		11	17864.735		12	17851.329		17859.4 [2]
3–5	12	16900.260		12	16901.808		13	16888.491		16901 [3]
3–6[a]						15949 [1]				
						15950 [2]				
4–0	8	22609.714		8	22610.389	22610 [2]	9	22598.630	22598 [2]	22608 [3]
4–1	10	21609.903		9	21610.534	21610 [2]	9	21598.807		21611 [3]
4–2	10	20619.300		10	20619.912		10	20608.153	20611 [2]	20624 [2]
										20621 [3]
4–3[a]	11	19637.898		10	19638.495		11	19626.797		
4–4[a]	11	18665.690		11	18666.320		11	18654.639		18655 [2]
4–5[a]	11	17702.743		11	17703.359		11	17691.749		
5–0[a]	8	23404.326		8	23402.807		7	23392.984		23413 [2]
5–1	8	22404.467		8	22402.937	22403 [2]	9	22393.112		22405 [3]
5–2	9	21413.793	21414 [2]	10	21412.258	20412 [2]	10	21402.472	20402 [2]	
5–3[a]	11	20432.387	20433 [2]	10	20430.841	20431 [2]	10	20421.063	20423 [2]	
5–4[a]	11	19460.179		10	19458.568		10	19448.840		
5–5[a]	11	18497.232		10	18495.551		11	18485.936		
6–0[a]				7	24185.806		8	24177.683		
6–1[a]				7	23185.891		8	23177.807		23169 [2]
6–2				9	22195.159	22196 [3]	9	22187.097	22187 [2]	
6–3				9	21213.672		9	21205.630		
6–4[a]				9	20241.353		10	20233.358		
6–5[a]				10	19278.337		10	19270.397		
7–0[a]	7	24954.533		7	24958.629		7	24952.632		
7–1[a]	7	23954.634		7	23958.714		8	23952.739		23951 [2]
7–2[a]	7	22963.885		7	22967.964		8	22962.022		22963 [2]
7–3	8	21982.354		8	21986.421	21986 [3]	8	21980.502	21981 [2]	
7–4[a]	10	21010.106		8	21014.077		10	21008.202	21008 [2]	21017 [2]
7–5[a]	10	20047.088		9	20050.967		10	20045.240		

Note. [1] 28Lowater (Lowater 1928), [2] 29Christya (Christy 1929a), [3] 72PhDa (Phillips & Davis 1972).
[a] MARVEL predicted band-heads.

fitted energies and the MARVEL energies; Schwenke himself reported an RMSE of $1.582\,\mathrm{cm^{-1}}$ between his fit and the experimental energy levels he used. This state is significantly affected by perturbations that are difficult to model theoretically and which have recently been analyzed by Namiki et al. (2003a).

Table 13
E $^3\Pi$ − X $^3\Delta$ R-branch Band-heads in cm^{-1} for ^{48}Ti^{16}O

| $v'-v''$ | E $^3\Pi_0$ − X $^3\Delta_1$ | | | E $^3\Pi_1$ − X $^3\Delta_2$ | E $^3\Pi_3$ − X $^3\Delta_3$ |
	J	MARVEL	Low-res obs.	Low-res obs.	Low-res obs.
0–0	26	11854.767	11856 [1]	11842 [1]	11828 [1]
0–1	32	10856.099	10857 [1]	10845 [1]	10831 [1]
1–0			12774 [1]	12760 [1]	12743 [1]
1–1[a]			11768 [1]	11753 [1]	11739 [1]
1–2[a]			10777 [1]	10766 [1]	10752 [1]
2–1[a]			12674 [1]	12658 [1]	12643 [1]
2–2[a]			11679 [1]	11667 [1]	11652 [1]
2–3[a]			10701 [1]	10689 [1]	10675 [1]
3–2[a]			12578 [1]	12564 [1]	12548 [1]
3–3[a]			11588 [1]	11576 [1]	11564 [1]
3–4[a]			10623 [1]	10607 [1]	10594 [1]
4–3[a]			12478 [1]	12462 [1]	12448 [1]
4–4[a]			11504 [1]	11487 [1]	11474 [1]
4–5[a]			10544 [1]	10521 [1]	10509 [1]
5–4[a]			12371 [1]	12356 [1]	12342 [1]

Note. [1] 77LiBr (Linton & Broida 1977a).
[a] MARVEL predicted band-heads.

Table 14
Singlet R-branch Band-heads in cm^{-1} for ^{48}Ti^{16}O

	$v'-v''$	J	MARVEL	Low-res obs.
b $^1\Pi$ − a $^1\Delta$	0–0	22	11284.109	
	0–1[a]	25	10276.404	10280 [1] 10282 [3]
	0–2[a]	28	9278.175	
	1–0	19	12194.027	12194 [2]
	1–1[a]	22	11185.966	11186 [1]
	1–2[a]	26	10187.226	10187 [1] 10191 [3]
	2–0[a]	17	13095.493	
	2–1[a]	19	12087.207	12092 [1]
	2–2[a]	22	11088.132	10099 [1] 10103 [3]
	3–0[a]	16	13988.405	
	3–1[a]	17	12979.947	
	3–2[a]	19	11980.629	11981 [1]
	3–4[a]			10011 [1], 10015 [3]
	4–0[a]	15	14872.663	
	4–1[a]	16	13864.061	
	4–2[a]	17	12864.569	
b $^1\Pi$ − d $^1\Sigma^+$	0–0	15	9061.930	9064 [1]
	0–1	16	8049.405	
	0–2	18	7046.835	7046.343 [6]
	0–3[a]	21	6054.266	
	0–4[a]	24	5071.780	
	0–5[a]	27	4099.283	
	1–0	14	9972.462	9972 [1], 9976 [3], 9972.424 [6]
	1–1	15	8959.784	8962 [1], 8959.789 [6]
	1–2	16	7957.084	7967.036 [6]
	1–3	18	6964.277	6964.220 [6]
	1–4[a]	21	5981.463	
	1–5[a]	24	5008.744	
	2–0	13	10874.420	10874.381 [6]
	2–1	14	9861.679	9867 [3], 9861.640 [6]
	2–2[a]	15	8858.820	
	2–3	17	7865.838	7865.786 [6]
	2–4[a]	19	6882.782	6882.550 [6]
	2–5[a]	21	5909.698	
	3–0[a]	12	11767.709	
	3–1	12	10754.909	10754.867 [6]

Table 14
(Continued)

	$v'-v''$	J	MARVEL	Low-res obs.
	3–2	14	9751.932	9756 [3], 9651.879 [6]
	3–3[a]	15	8758.826	
	3–4	17	7775.659	7775.519 [6]
	3–5[a]	19	6802.248	6802.185 [6]
	4–0[a]	11	12652.286	
	4–1[a]	11	11639.391	
	4–2	13	10636.341	10636.312 [6]
	4–3	14	9643.116	9643.049 [6]
	4–4[a]	15	8659.749	
	4–5[a]	16	7686.202	
c $^1\Phi$ − a $^1\Delta$	0–0	36	17859.641	17859 [4]
	0–1[a]	46	16855.359	
	1–0[a]	30	18765.794	18767 [5]
	1–1	36	17759.615	17759 [4]
	1–2[a]	44	16763.966	16770 [4]
	2–0[a]	24	19662.833	
	2–1[a]	29	18655.669	18658 [5]
	2–2	35	17658.308	17658 [4]
	3–2[a]			18549 [5]
	3–3			17556 [4]
	3–4[a]			16566 [4]
	4–3[a]			18438 [5]
	4–4[a]			17455 [4]
f $^1\Delta$ − a $^1\Delta$	0–0;	15	19076.916	19075.4 [7]
	0–1[a]	17	18068.396	18068.4 [7]
	0–2[a]	18	17069.021	17072.1 [7]
	1–0[a]	14	19945.353	
	1–1	15	18936.706	18918.3 [7]
	1–2[a]	17	17937.144	17918.7 [7]
	2–0[a]	14	20809.072	
	2–1[a]	14	19800.392	19785.5 [7]
	2–2	17	18800.792	18763.9 [7]
	2–3			17775.9 [7]
e $^1\Sigma^+$ − d $^1\Sigma^+$	0–0	9	24302.257	
	0–1[a]	9	23289.220	
	0–2[a]	9	22285.939	
	0–3[a]	11	21292.407	
	0–4[a]	11	20308.720	
	0–5[a]	12	19334.758	
	1–0	9	25146.767	
	1–1[a]	10	24133.737	
	1–2[a]	10	23130.521	
	1–3[a]	10	22137.051	
	1–4[a]	10	21153.289	
	1–5[a]	10	20179.273	

Note. [1] 37WuMe (Wurm & Meister 1937), [2] 57GaRoJu (Gatterer et al. 1957), [3] 69Lockwood (Lockwood 1969), [4] 28Lowater (Lowater 1928), [5] 69LiNi (Linton & Nicholls 1969), [6] 80GaBrDa (Galehouse et al. 1980), [7] 82DeVore (DeVore 1982).
[a] MARVEL predicted band-heads.

Figure 5 compares the MARVEL experimentally derived energy levels and the fitted energy levels used in the Schwenke (1998) line list for singlet states. The d $^1\Sigma^+$, a $^1\Delta$, c $^1\Phi$, and f $^1\Delta$ levels seem reasonable; the deviation from the fitted Schwenke lines increases for larger J in general. However, errors for the b $^1\Pi$ state are particularly high, around 3 cm^{-1}. Schwenke reports an RMSE of 0.054 cm^{-1}. However, our predicted b $^1\Pi$–d $^1\Sigma^+$ band-heads reproduce experiment almost
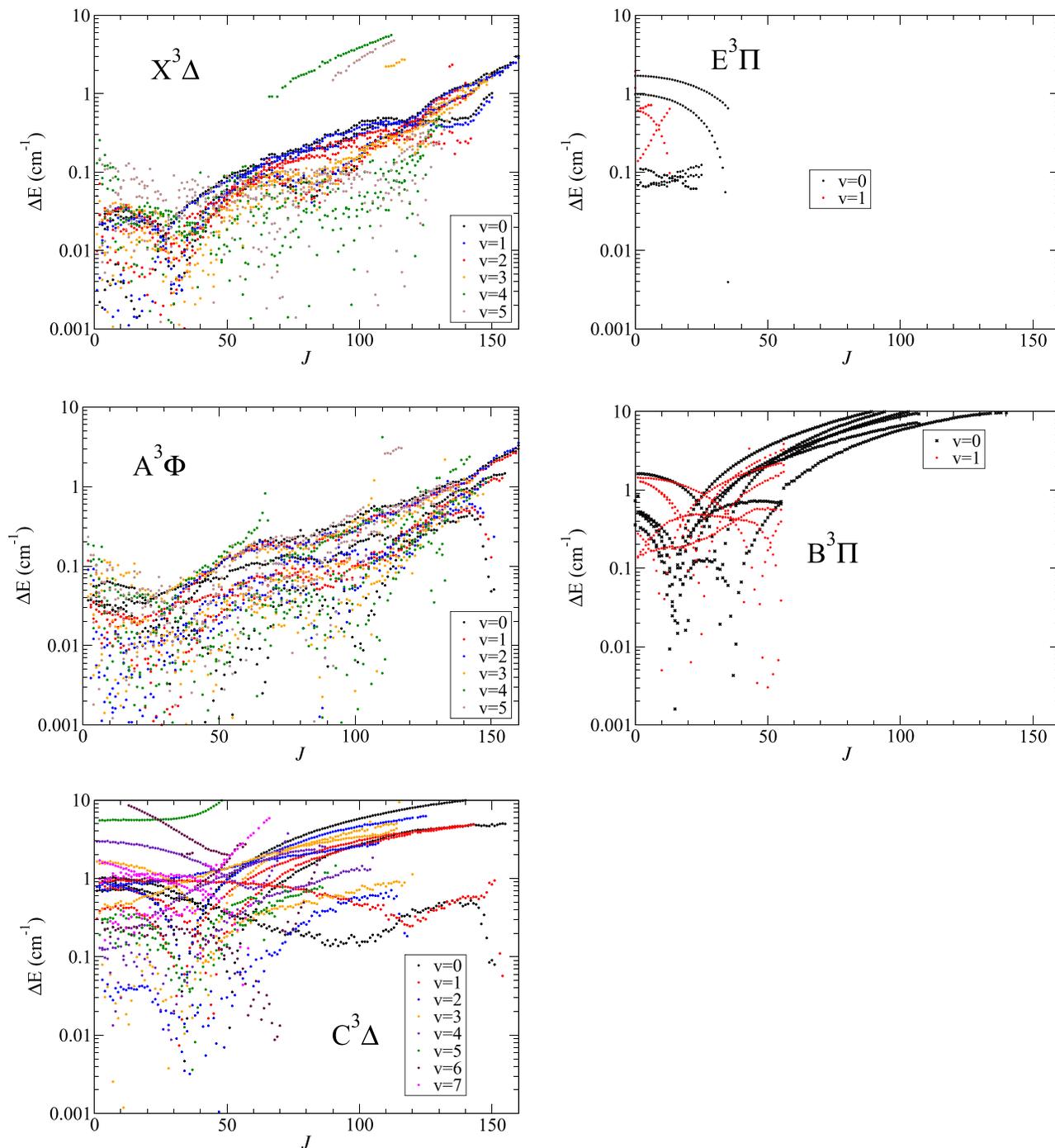
Figure 4. Visual comparison of the absolute energy difference between the MARVEL experimentally derived energy levels and those in the Schwenke (1998) line list for triplet states. Note the logarithmic vertical axis.

perfectly, whereas there are clear discrepancies between experiment and the Schwenke data (see Figure 6). We therefore conclude that there is an approximately 3 cm^{-1} off-set error in the b $^1\Pi$ state Schwenke energy levels.

4.5. Comparison with VALD

Figures 7 and 8 show a visual comparison of the 2012 version of the Plez TiO line list from the VALD database (Ryabchikova et al. 2015) versus MARVEL energy levels for the triplet and singlet states, respectively. For the triplets, we get results

qualitatively similar to the Schwenke comparisons, though the errors are often about a factor of 10 larger (note the difference in the vertical scale between the Plez and Schwenke comparisons). However, for the singlets, it is clear that the vibrational spacings within some singlet states are incorrect. The Phillips experimental frequencies (for which the most recent version of this line list is fitted) may have been correctly reproduced. However, other experimental data would not be, due to these erroneous vibrational frequencies. The MARVEL energies will thus allow a more thorough understanding of the whole spectrum of TiO.
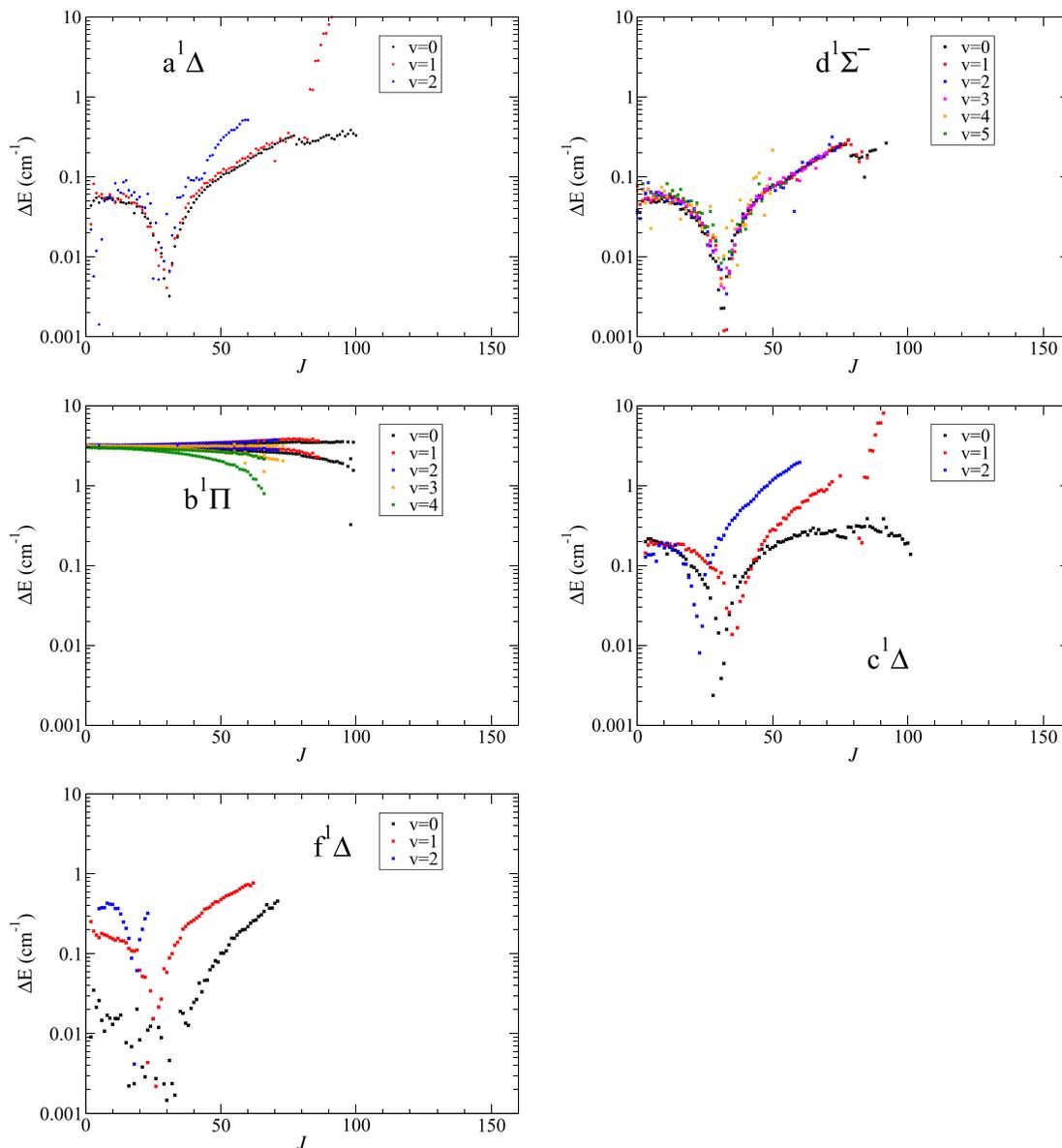
Figure 5. Visual comparison of the absolute energy difference between the MARVEL experimentally derived energy levels and those in the Schwenke (1998) line list for singlet states. Note the logarithmic vertical axis.

4.6. Future Directions

4.6.1. Recommended Experiments

The experimental coverage of rovibronic bands in TiO is extensive. However, the complexity of the electronic structure of this species and its importance in understanding, modeling, and interpreting the spectroscopy and opacity of cool stars and hot-Jupiter exoplanets means that extra experimental data are always welcome. We would like to direct experimentalists toward some key transitions for which data are not yet available and for which our experience with ab initio computations (Lodi et al. 2015; McKemmish et al. 2016a; Tennyson et al. 2016a; M. Gorman et al. 2017, in preparation) on these species leads us to conclude that they will not be computed to satisfactory accuracy.

The D $^3\Sigma^-$ state has been identified by Barnes et al. (1997) using fluorescence from a very high $^3\Pi$ state but its spectrum has not been rotationally resolved or measured with high
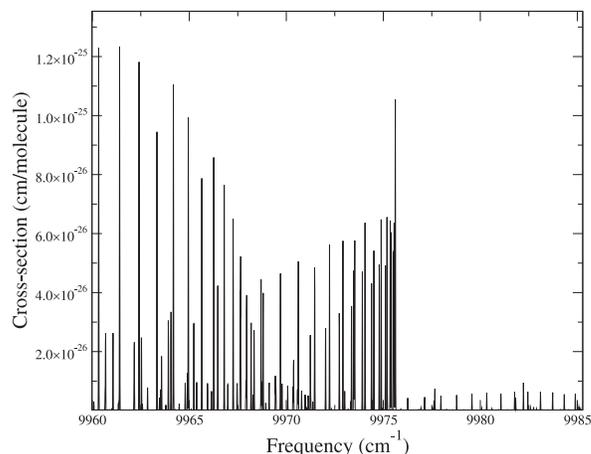
Figure 6. Simulated absorption cross-section from the Schwenke (1998) line list at 300 K, $\delta\nu = 0.01$ cm^{-1}. The b $^1\Pi$–d $^1\Sigma^+$ (1–0) bandhead experimentally is 9972.42 cm^{-1} (Galehouse et al. 1980).
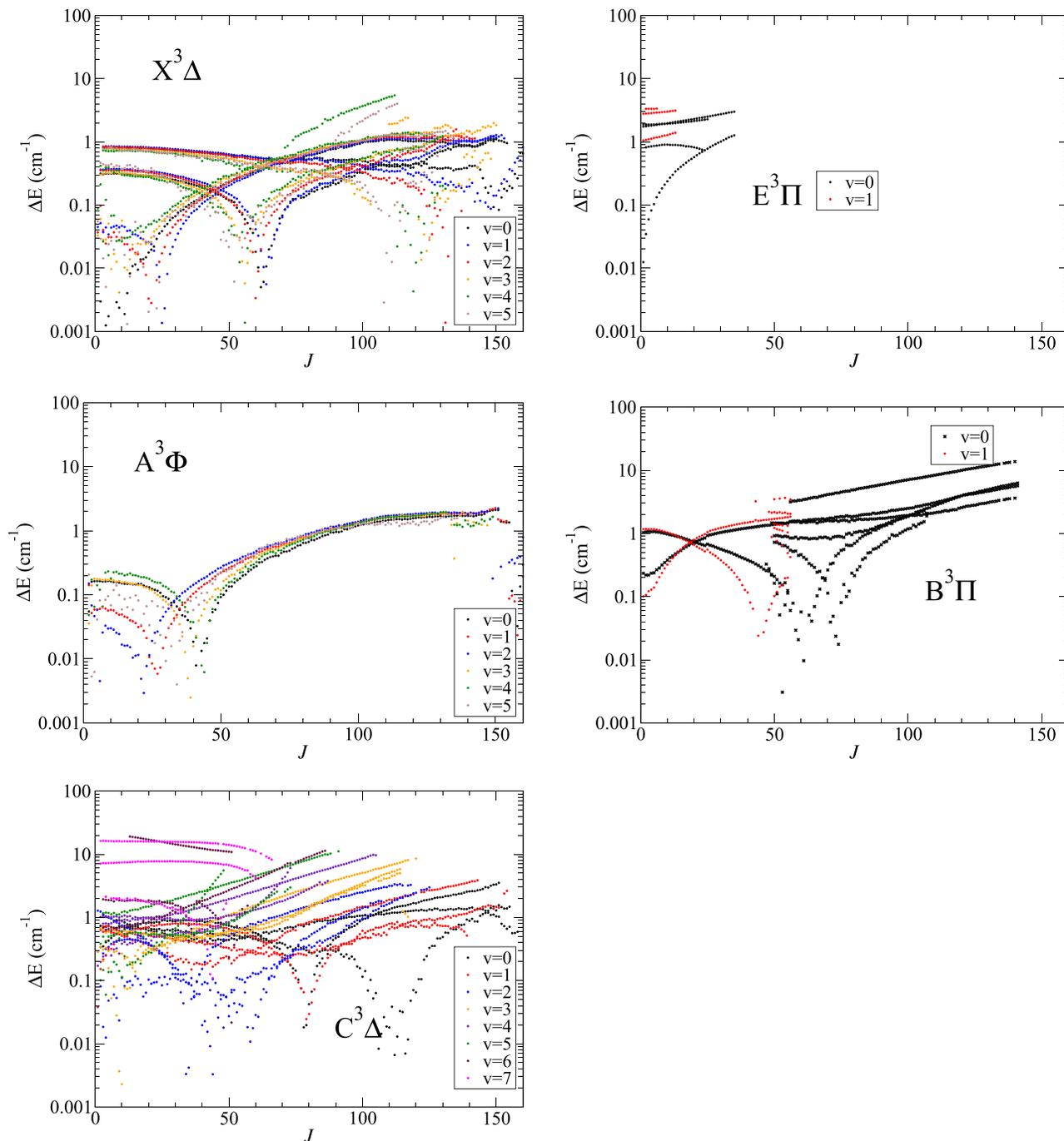
Figure 7. Visual comparison of the absolute energy difference between the MARVEL experimentally derived energy levels and those in the Plez (1998) line list for triplet states. Note the logarithmic vertical axis and that the axis range is different from Figure 4.

accuracy. For the purposes of absorption spectroscopy of astrophysical objects, further data are probably not critical as this state does not contribute to any allowed absorption bands from the electronic states with significant thermal population at 5000 K, nor does it appear to be a strong perturber of the other states. However, it will contribute to weak background absorption and, more importantly, the partition function of TiO.

Rotationally resolved data involving higher vibrational excitations of the B $^3\Pi$ and E $^3\Pi$ electronic states are both achievable (given the detection of band-heads), and valuable for constraining the shape of the potential energy curves of these states.

Hints from experimental observations, e.g., $^1\Pi$ state near 22,300 cm^{-1} by Namiki et al. (2003a), ab initio evidence and results from similar diatomic species strongly suggest that experimental identification of electronic states between 20,000 cm^{-1} and 30,000 cm^{-1} is not complete for singlet states. Targeted (non-absorption) experiments, perhaps two-photon ones, are probably required to map out this region more thoroughly. This means that understanding ^{48}Ti^{16}O absorption in the UV and bluer region of the visible spectra may be currently incomplete. This is of most relevance to transit spectroscopy of hot Jupiters around stars with strong UV fluxes.
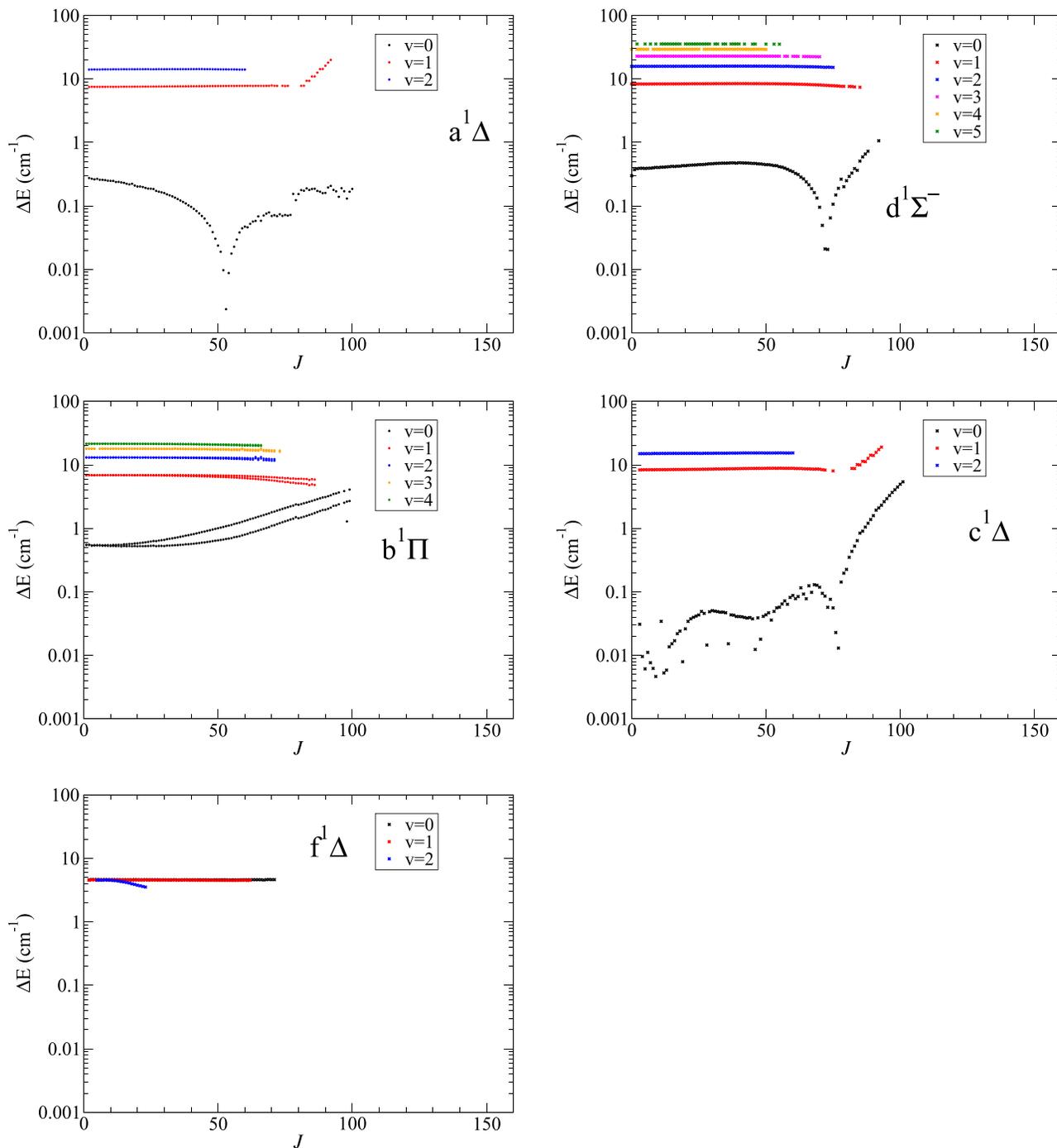
Figure 8. Visual comparison of the absolute energy difference between the MARVEL experimentally derived energy levels and those in the Plez (1998) line list for singlet states. Note the logarithmic vertical axis and that the axis range is different from Figure 5.

5. Conclusions

We have collated all suitable available assigned TiO experimental data. We have used over 48,000 assigned transitions to produce 10,564 energy levels. These span 11 electronic states, and 84 total rovibronic bands.

This paper contains the data.tar.gz supplemental package. It contains the file 48Ti-16O_FFN_ca_33.energies, which contains the relative energies in the free-floating network incorporating the c $^1\Phi$ $v = 3$ and a $^1\Delta$ $v = 3$ states, and three directories containing sorted folders and files with predicted transition frequencies using the MARVEL energies.

The data collated here assists with the evaluation of the partition function for ^{48}Ti^{16}O. However, there are two other electronic states, the D $^3\Sigma^-$ and g $^1\Gamma$ states, which high-quality theory (Miliordos & Mavridis 2010) predicts exist below 20,000 cm^{-1} that have not been experimentally characterized in rotationally resolved spectra. Furthermore, in many cases, only a small number of vibrational levels have MARVEL data. Therefore, we will defer the detailed evaluation of an updated recommended partition function for the upcoming ^{48}Ti^{16}O line-list paper (L. K. McKemmish et al. 2017, in preparation) that will produce an extensive spectroscopic model incorporating a

large number of vibrational levels in all low-lying electronic states of $^{48}Ti^{16}O$.

The MARVEL energy level data is going to be immediately useful in the construction of the new ExoMol line list for TiO (L. K. McKemmish et al. 2017, in preparation). The energy levels presented here will allow the accurate refinement of the potential energy curves and coupling constants, i.e., the spectroscopic model, in order to maximize the quality of the predicted energy levels. The refinement process is particularly important for transition metal diatomics due to the complexity of the electronic states and the insufficient accuracy of even modern ab initio methods (Tennyson et al. 2016a).

Finally, we note that a major part of this work was performed by 16 and 17 year old pupils from the Highams Park School in London, as part of a project known as ORBYTS (Original Research By Young Twinkle Students). Two other MARVEL studies on astronomically important molecules, methane (E. Barton et al. 2017, in preparation) and acetylene (K. Chubb et al. 2017, in preparation), were undertaken as part of the same project and will be published elsewhere. C. Sousa-Silva et al. (2017, in preparation) discusses our experiences of working with school children to perform high-level research.

References

Al Derzi, A. R., Furtenbacher, T., Yurchenko, S. N., Tennyson, J., & Császár, A. G. 2015, JQSRT, 161, 117
Allard, F., Hauschildt, P. H., Miller, S., & Tennyson, J. 1994, ApJL, 426, L39
Allard, F., Hauschildt, P. H., & Schwenke, D. 2000, ApJ, 540, 1005
Amiot, C., Azaroual, E. M., Luc, P., & Vetter, R. 1995, JChPh, 102, 4375
Amiot, C., Cheikh, M., Luc, P., & Vetter, R. 1996, JMoSp, 179, 159
Amiot, C., Luc, P., & Vetter, R. 2002, JMoSp, 214, 196
Árendás, P., Furtenbacher, T., & Császár, A. G. 2016, JMaCh, 54, 806
Balducci, G., Guido, M., Piacente, V., & Demaria, G. 1972, JChPh, 56, 3422
Barber, R. J., Strange, J. K., Hill, C., et al. 2014, MNRAS, 437, 1828
Barnes, M., Merer, A. J., & Metha, G. F. 1996, JMoSp, 180, 437
Barnes, M., Merer, A. J., & Metha, G. F. 1997, JMoSp, 181, 180
Bernath, P. F. 2016, Spectra of Atoms and Molecules (3rd ed.; Oxford: Oxford Univ. Press)
Birge, R., & Christy, A. 1927, PhRv, 2, 212
Brandes, G. R., & Galehouse, D. C. 1985, JMoSp, 109, 345
Brom, J. M., & Broida, H. P. 1975, JChPh, 63, 3718
Brown, J. M., Hougen, J. T., Huber, K. P., et al. 1975, JMoSp, 55, 500
Budo, A. 1936, ZPhy, 98, 437
Carette, P., & Schamps, J. 1992, JMoSp, 154, 448
Carlson, R. C., Cross, L. A., & Dunn, T. M. 1985, CPL, 113, 515
Christy, A. 1929a, PhRv, 33, 701

Christy, A. 1929b, ApJ, 70, 1
Christy, A., & Birge, R. 1928, Natur, 122, 205
Colibaba-Evulet, A., Singhal, A., & Glumac, N. 2000, CST, 157, 129
Collins, J. G. 1975a, PhD thesis, Indiana Univ.
Collins, J. G. 1975b, JPhB, 8, 304
Collins, J. G., & Fay, D. J. 1976, JQSRT, 14, 1259
Császár, A. G., Czakó, G., Furtenbacher, T., & Mátyus, E. 2007, Annual Reports in Computational Chemistry, 3, 155
Császár, A. G., & Furtenbacher, T. 2011, JMoSp, 266, 99
Császár, A. G., & Furtenbacher, T., & Árendás, P. 2016, JPCA, 120, 8949
Davis, S. P., Littleton, J. E., & Phillips, J. G. 1986, ApJ, 309, 449
de Kok, R. J., Birkby, J., Brogi, M., et al. 2014, A&A, 561, A150
Desert, J. M., Vidal-Madjar, A., des Etangs, A. L., et al. 2008, A&A, 492, 585
DeVore, T. C. 1982, HTemS, 15, 219
Dobronravin, P. P. 1937, C.R. Acad. Sci. URSS, 17, 399
Doverstal, M., & Weijnitz, P. 1992, MolPh, 75, 1357
Dube, P. S. 1972, IJPAP, 10, 70
Dubois, L. H., & Gole, J. L. 1977, JChPh, 66, 779
Dyke, J. M., Gravenor, B. W. J., Josland, G. D., Lewis, R. A., & Morris, A. 1984, MolPh, 53, 465
Engvold, O. 1973, A&AS, 10, 11
Evans, T. M., Sing, D. K., Wakeford, H. R., et al. 2016, ApJL, 822, L4
Fábri, C., Mátyus, E., Furtenbacher, T., et al. 2011, JChPh, 135, 094307
Fairbairn, A. R., Wolnik, S. J., & Berthel, R. O. 1974, ApJ, 193, 273
Feinberg, J., Bilal, M. G., Davis, S. P., & Phillips, J. G. 1976, ApL, 17, 147
Feinberg, J., & Davis, S. P. 1977, JMoSp, 65, 264
Feinberg, J., & Davis, S. P. 1978, JMoSp, 69, 445
Fletcher, D. A., Scurlock, C. T., Jung, K. Y., & Steimle, T. C. 1993, JChPh, 99, 4288
Fortney, J. J., Lodders, K., Marley, M. S., & Freedman, R. S. 2008, ApJ, 678, 1419
Fortney, J. J., Robinson, T. D., Domagal-Goldman, S., et al. 2016, White Paper Originally Initiated Within NASA's Nexus for Exoplanet System Science (NExSS), with Additional Community Input, arXiv:1602.06305
Fowler, A. 1904, RSPSA, 73, 219
Furtenbacher, T., Árendás, P., Mellau, G., & Császár, A. G. 2014, NatSR, 4, 4654
Furtenbacher, T., & Császár, A. G. 2012a, JMoSp, 1009, 123
Furtenbacher, T., & Császár, A. G. 2012b, JQSRT, 113, 929
Furtenbacher, T., Császár, A. G., & Tennyson, J. 2007, JMoSp, 245, 115
Furtenbacher, T., Szabo, I., Császár, A. G., et al. 2016, ApJS, 224, 44
Furtenbacher, T., Szidarovszky, T., Fábri, C., & Császár, A. G. 2013a, PCCP, 15, 10181
Furtenbacher, T., Szidarovszky, T., Mátyus, E., Fábri, C., & Császár, A. G. 2013b, Journal of Chemical Theory and Computation, 9, 5471
Galehouse, D. C., Brault, J. W., & Davis, S. P. 1980, ApJS, 42, 241
Gallaher, T. N., & DeVore, T. C. 1979, HTemS, 11, 123
Gatterer, A., Rosen, B., Junkes, J., & Salpeter, E. W. 1957, Molecular Spectra of Metallic Oxides (Rome: Specola Vaticana)
Gustavsson, T., Amiot, C., & Verges, J. 1991, JMoSp, 145, 56
Haynes, K., Mandell, A. M., Madhusudhan, N., Deming, D., & Knutson, H. 2015, ApJ, 806, 146
Hedgecock, I. M., Naulin, C., & Costes, M. 1995, A&A, 304, 667
Hermann, J., Perrone, A., & Dutouquet, C. 2001, JPhB, 34, 153
Hildenbrand, D. L. 1976, CPL, 44, 281
Hocking, W. H., Gerry, M. C. L., & Merer, A. J. 1979, CaJPh, 57, 54
Hoeijmakers, H. J., de Kok, R. J., Snellen, I. A. G., et al. 2015, A&A, 575, A20
Huang, H., Luo, Z., Chang, Y. C., Lau, K.-C., & Ng, C. 2013, JChPh, 138, 174309
Huitson, C. M., Sing, D. K., Pont, F., et al. 2013, MNRAS, 434, 3252
Jorgensen, U. G. 1994, A&A, 284, 179
Kaledin, L. A., McCord, J. E., & Heaven, M. C. 1995, JMoSp, 173, 499
King, A. S. 1926, PASP, 38, 173
Kobayashi, K., Hall, G. E., Muckerman, J. T., Sears, T. J., & Merer, A. J. 2002, JMoSp, 212, 133
Kobylyansky, A. I., Kulikov, A. N., & Gurvich, L. V. 1983, OpSp, 54, 433
Lindgren, B. 1972, JMoSp, 43, 474
Linton, C. 1972, CaJPh, 50, 312
Linton, C. 1974, JMoSp, 50, 235
Linton, C., & Broida, H. P. 1977a, JMoSp, 64, 382
Linton, C., & Broida, H. P. 1977b, JMoSp, 64, 389
Linton, C., & Nicholls, R. 1969, JPhB, 2, 490
Linton, C., & Nicholls, R. W. 1970, JQSRT, 10, 311
Linton, C., & Singhal, S. R. 1974, JMoSp, 51, 194
Lockwood, G. 1969, ApJ, 157, 275
Lodders, K. 2002, ApJ, 577, 974

Lodi, L., Yurchenko, S. N., & Tennyson, J. 2015, MolPh, 113, 1559
Lowater, F. 1928, PPS, 41, 557
Lowater, F. 1929, Natur, 123, 644
Luc, P., d'Aignaux, Y., Amiot, C., & Vetter, R. 1997, Metro, 34, 319
Lundevall, C. 1998, JMoSp, 191, 93
Makita, M. 1968, SoPh, 3, 557
McIntyre, N. S., Thompson, K. R., & Weltner, W., Jr. 1971, JPhCh, 75, 3243
McKemmish, L. K., Yurchenko, S. N., & Tennyson, J. 2016a, MolPh, 114, 3232
McKemmish, L. K., Yurchenko, S. N., & Tennyson, J. 2016b, MNRAS, 463, 771
Miliordos, E., & Mavridis, A. 2010, JPCA, 114, 8536
Mulliken, R. S. 1955, JChPh, 23, 1997
Namiki, K., Saito, S., Robinson, J. S., & Steimle, T. C. 1998, JMoSp, 191, 176
Namiki, K. C., Ito, H., & Davis, S. P. 2003a, JMoSp, 217, 173
Namiki, K. C., Miki, H., & Ito, H. 2003b, CPL, 370, 62
Namiki, K. C., Saitoh, H., & Ito, H. 2004, JMoSp, 226, 87
Nikolov, N., Sing, D. K., Burrows, A. S., et al. 2015, MNRAS, 447, 463
Palmer, H. B., & Hsu, C. J. 1972, JMoSp, 43, 320
Pathak, C. M., & Palmer, H. B. 1970, JMoSp, 33, 137
Paulose, G., Barton, E. J., Yurchenko, S. N., & Tennyson, J. 2015, MNRAS, 454, 1931
Pettersson, A. 1959a, ArMAF, 16, 185
Pettersson, A., & Lindgren, B. 1962, ArMAF, 22, 491
Pettersson, A. V. 1959b, NW, 46, 200
Pettersson, A. V., & Lindgren, B. 1961, NW, 48, 128
Phillips, J. G. 1950, ApJ, 111, 314
Phillips, J. G. 1951, ApJ, 114, 152
Phillips, J. G. 1952, ApJ, 115, 567
Phillips, J. G. 1952, ApJ, 115, 183
Phillips, J. G. 1954, ApJ, 119, 274
Phillips, J. G. 1969, ApJ, 157, 449
Phillips, J. G. 1971, ApJ, 169, 185
Phillips, J. G. 1973, ApJS, 26, 313
Phillips, J. G. 1974, ApJS, 27, 319
Phillips, J. G., & Davis, S. P. 1971, ApJ, 167, 209
Phillips, J. G., & Davis, S. P. 1972, ApJ, 175, 583
Plez, B. 1992, A&AS, 94, 527

Plez, B. 1998, A&A, 337, 495
Price, M., Sulzmann, K., & Penner, S. 1971, JQSRT, 11, 427
Price, M. L., Sulzmann, K. G., & Penner, S. S. 1974, JQSRT, 14, 1273
Ram, R. S., Bernath, P. F., Dulick, M., & Wallace, L. 1999, ApJS, 122, 331
Ram, R. S., Bernath, P. F., & Wallace, L. 1996, ApJS, 107, 443
Rao, V. M., Rao, M. L. P., & Rao, P. T. 1979, SpecL, 12, 887
Ryabchikova, T., Piskunov, N., Kurucz, R. L., et al. 2015, PhyS, 90, 054005
Schwenke, D. W. 1998, FaDi, 109, 321
Simard, B., & Hackett, P. A. 1991, JMoSp, 148, 128
Sing, D. K., Fortney, J. J., Nikolov, N., et al. 2016, Natur, 529, 59
Sing, D. K., Lecavelier des Etangs, A., Fortney, J. J., et al. 2013, MNRAS, 436, 2956
Steele, R. E., & Linton, C. 1978, JMoSp, 69, 66
Steimle, T. C., & Shirley, J. E. 1989, JChPh, 91, 8000
Steimle, T. C., Shirley, J. E., Jung, K. Y., Russon, L. R., & Scurlock, C. T. 1990, JMoSp, 144, 27
Steimle, T. C., & Virgo, W. 2003, CPL, 381, 30
Tennyson, J., Bernath, P. F., Brown, L. R., et al. 2009, JQSRT, 110, 573
Tennyson, J., Bernath, P. F., Brown, L. R., et al. 2010, JQSRT, 111, 2160
Tennyson, J., Bernath, P. F., Brown, L. R., et al. 2013, JQSRT, 117, 29
Tennyson, J., Bernath, P. F., Brown, L. R., et al. 2014a, Pure Appl. Chem., 86, 71
Tennyson, J., Bernath, P. F., Brown, L. R., et al. 2014b, JQSRT, 142, 93
Tennyson, J., Lodi, L., McKemmish, L. K., & Yurchenko, S. N. 2016a, JPhB, 49, 102001
Tennyson, J., Yurchenko, S. N., Al-Refaie, A. F., et al. 2016b, JMoSp, 327, 73

Vetter, R., Luc, P., & Amiot, C. 1998, Laser Chemistry, 18, 1
Virgo, W. L., Steimle, T. C., & Brown, J. M. 2005, ApJ, 628, 567
Watson, J. K. G. 2003, JMoSp, 219, 326
Williamson, B. E., Roser, D. C., & Vala, M. 1994, JPhCh, 98, 3624
Woods, A. C., Parigger, C. G., & Hornkohl, J. O. 2012, OptL, 37, 5139
Wurm, K., & Meister, H.-J. 1937, ZA, 13, 199
Yurchenko, S. N., Lodi, L., Tennyson, J., & Stolyarov, A. V. 2016, CoPhC, 202, 262
Zyrnicki, W. 1975, JQSRT, 15, 575
Zyrnicki, W., & Palmer, H. B. 1976, PhyBC, 84, 152